A comprehensive experimental and modeling study of isobutene oxidation

Chong-Wen Zhou, Yang Li, Eoin O'Connor, Kieran P Somers, Sébastien
Thion, Charles Keesee, Olivier Mathieu, Eric L Petersen, Trent A Deverter,
Matthew A. Oehlschlaeger, et al.

A COMPREHENSIVE EXPERIMENTAL AND MODELING STUDY OF ISOBUTENE OXIDATION

Chong-Wen Zhou[a], Yang Li[a], Eoin O'Connor[a], Kieran P. Somers[a], Sébastien Thion[b], Charles Keesee[b], Olivier Mathieu[b,], Eric L. Petersen[b], Trent A. DeVerter[c], Matthew A. Oehlschlaeger[c], Goutham Kukkadapu[d], Chih-Jen Sung[d], Majed Alrefae[e], Fathi Khaled[e], Aamir Farooq[e], Patricia Dirrenberger[f], Pierre-Alexandre Glaude[f], Frédérique Battin-Leclerc[f], Jeffrey Santner[g], Yiguang Ju[g,h], Timothy Held[g], Francis M. Haas[g], Frederick L. Dryer[g], Henry J. Curran[a]

[a]Combustion Chemistry Centre, National University of Ireland Galway, Ireland. [b]Department of Mechanical Engineering, Texas A&M University, College Station, TX, United States. [c]Department of Mechanical, Aerospace, and Nuclear Engineering, Rensselaer Polytechnic Institute, Troy, NY, United States. [d]Department of Mechanical Engineering, University of Connecticut, CT, United States. [e]Clean Combustion Research Center, King Abdullah University of Science and Technology, Thuwal, Saudi Arabia. [f]Laboratoire Réactions et Génie des Procédés, CNRS-Université de Lorraine, Nancy, France. [g]Department of Mechanical and Aerospace Engineering, Princeton University, Princeton, NJ, United States. [h]Current address: Argonne National Laboratory, Argonne, United States.

Abstract

Isobutene is an important intermediate in the pyrolysis and oxidation of higher-order branched alkanes, and is a component of commercial gasoline and diesel fuels. To better understand its combustion characteristics, a series of ignition delay times (IDTs) and laminar flame speed (LFS) measurements have been performed. In addition, speciation data recorded in a flow reactor for the pyrolysis and oxidation of isobutene is also reported.

IDTs of isobutene oxidation were measured in four different shock tubes and in two rapid compression machines (RCMs) under conditions of relevance to practical combustors. The combination of shock tube and RCM data greatly expands the range of available validation data for isobutene oxidation models to pressures of 50 atm and temperatures in the range 666–1715 K. Isobutene flame speeds were measured experimentally at 1 atm and at unburned gas temperatures of 298–398 K over a wide range of equivalence ratios. For the flame speed results, there was good agreement between different facilities and the current model in the fuel-rich region.

Ab initio chemical kinetics calculations were carried out to calculate rate constants for important reactions such as H-atom abstraction by hydroxyl and hydroperoxyl radicals and the decomposition of 2-methylallyl radicals. The M062X/6-311++G(d,p) method was used in the geometry optimizations, frequency calculations and potential energy surface scans for the individual hindered rotors. The electronic single point energies were calculated at the QCISD(T)/CBS level of theory. Conventional transition-state theory with an asymmetric Eckart tunneling correction was used to calculate the high-pressure limit rate constants in this work. The low-frequency torsional conserved modes were treated as hindered rotors using a Pitzer-Gwinn-like approximation to calculate the partition function.

A comprehensive chemical kinetic mechanism has been developed to describe the combustion of isobutene and is validated by comparison to the present IDT, LFS and flow-reactor speciation measurements. Important reactions, highlighted via flux and sensitivity analyses, include: (a) hydrogen atom abstraction from isobutene by hydroxyl and hydroperoxyl radicals, and molecular oxygen; (b) radical–radical recombination reactions, including 2-methylallyl radical self-

recombination, the recombination of 2-methylallyl radicals with hydroperoxyl radicals; and the recombination of 2-methylallyl radicals with methyl radicals; (c) addition reactions, including hydrogen atom and hydroxyl radical addition to isobutene; and (d) 2-methylallyl radical decomposition reactions. The current mechanism accurately predicts the ignition delay times and flame speed measurements presented in this study and also for jet-stirred reactor and flow reactor speciation data already available in the literature.

The differences in low-temperature chemistry between alkanes and alkenes are also highlighted in this work. In normal alkanes, the fuel radical $\dot{R}$ adds to molecular oxygen forming alkylperoxyl ($R\dot{O}_2$) radicals followed by isomerization and chain branching reactions which promote low-temperature fuel reactivity. However, in alkenes, because of the relatively shallow well (~20 kcal mol^{-1}) for $R\dot{O}_2$ formation compared to ~35 kcal mol^{-1} in alkanes, the $\dot{R} + O_2 \rightleftharpoons R\dot{O}_2$ equilibrium lies more to the left favoring $\dot{R} + O_2$ rather than $R\dot{O}_2$ radical stabilization. Based on this work, and related studies of allylic systems, it is apparent that reactivity for alkene components at very low temperatures (< 800 K) emanates from hydroxyl radical addition followed by radical addition to molecular oxygen. At intermediate temperatures (800–1300 K), alkene reactivity is controlled by hydrogen abstraction by molecular oxygen and the reactions between resonantly stabilized radicals and hydroperoxyl radicals which results in chain branching. At higher temperatures (> 1300 K), the reactivity is mainly governed by the competition between hydrogen abstractions by molecular oxygen and $\dot{O}H$ radicals.

Keywords: Isobutene oxidation, shock tube, rapid compression machine, chemical kinetics, ignition, flame speed, *ab initio*

1. Introduction

Isobutene, one of the butene isomers, is a known component of transportation fuels, as well as being an important intermediate in the pyrolysis and oxidation of higher-order branched hydrocarbons such as isooctane. The pyrolysis and oxidation of ethyl *tertiary*-butyl ether, used worldwide as an octane enhancer, also produces a significant amount of isobutene. Therefore, kinetic modeling of the combustion of commercial fuels requires a reliable computational tool that can predict the pyrolysis and oxidation behaviors of isobutene and similar compounds (1- and 2-butene). Serving as an archetypal alkene fuel, isobutene is also a precursor for soot formation. Following H-atom abstraction from isobutene, a resonantly stabilized 2-methylallyl radical is formed. Allylic species are implicated in the formation of aromatic and subsequent poly-aromatic hydrocarbon species [1]; therefore, understanding the oxidation chemistry of isobutene is important in helping mitigate pollutant formation.

Moreover, understanding the combustion chemistry of the butene isomers is a prerequisite for a comprehensive description of the chemistry of C1–C4 hydrocarbon and oxygenated fuels. For the development and validation of combustion models, it is thus crucial to improve our knowledge of detailed C4 combustion chemistry. Building a comprehensive kinetic model for isobutene is also an extension of our work on propene [2, 3].

Several research groups have investigated isobutene pyrolysis and oxidation in shock tubes [4-10], a turbulent flow reactor [11], a jet-stirred reactor [12] and in premixed laminar flames [13-15]. Yasunaga et al. [9] investigated the pyrolysis and oxidation of isobutene behind reflected shock waves over a temperature range of 1000–1800 K, measuring the product distribution using infrared laser absorption spectroscopy and gas-chromatography. The authors reported species profiles for CH_4 (methane), C_2H_6 (ethane), C_2H_2 (acetylene), C_3H_4-p (propyne), C_3H_4-a (allene), C_3H_6 (propene), 1,3-C_4H_6 (1,3-butadiene) and C_6H_6 (benzene).

Bauge *et al.*[4] measured ignition delay times of between 3 ms and 760 ms in the temperature range of 1230–1930 K over the pressure range of 9.5–10.5 atm for isobutene/oxygen mixtures containing 74.45–98.5% argon diluent. They also measured speciation data in a continuous-flow stirred-tank reactor at 1 atm in the temperature range 833–913 K. Curran [10] measured ignition delay times for isobutene/oxygen mixtures containing 80.8–98.8% argon diluent in the temperature range 1200–1980 K and at pressures in the range 2.2–4.5 atm.

Dias and Vandooren [13] studied a lean, premixed isobutene/hydrogen/oxygen/argon flame ($\phi = 0.225$) using molecular beam mass spectrometry at low pressure (40 mbar). They reported the following detected species: H_2, $\dot{C}H_3$, $\ddot{O}$, $\dot{O}H$, $H\dot{O}_2$, H_2O, C_2H_2 (acetylene), CO, C_2H_4 (ethylene), CH_2O (formaldehyde), O_2, Ar, C_3H_6 (propene), CO_2, CH_3CHO (acetaldehyde), 1,3-C_4H_6 (1,3-butadiene), iC_4H_8 (isobutene), C_3H_6O (acetone), C_4H_6O (1-propen-1-one, 2-methyl) and tautomers of isobutanal (C_4H_8O, prop-1-en-1-ol, 2-methyl and propanal, 2-methyl).

There have been several kinetic mechanisms published in the literature that can be used to simulate isobutene combustion [12, 14-16]. Dagaut and co-workers [12] studied the oxidation of isobutene in a jet-stirred reactor at high temperature (~800–1230 K) and at 1, 5 and 10 atm and reported species profiles as a function of temperature. Molecular species concentration profiles of O_2, H_2, CO, CO_2, CH_2O, CH_4, C_2H_2, C_2H_4, C_2H_6, C_3H_4 (allene and propyne), C_3H_6, acetone, acrolein, methacrolein, 1-C_4H_8, i-C_4H_8, 1,3-C_4H_6, 1-butyne, 2-methyl-1-butene, 2-methyl-2-butene, and benzene were obtained by probe sampling and gas chromatographs (GC) analysis. They also presented a chemical kinetic reaction mechanism capable of reproducing their speciation results. Zhang *et al*. [16] developed a model to describe the pyrolysis of the butene isomers in the temperature range 900–1900 K at low pressures (~7.5–12.5 Torr), in which kinetic data for the thermal decomposition of butene isomers was

proposed and recently adopted in the kinetic model of isomeric butanols by Cai *et al*. [17]. Schenk *et al*. [14] developed a high-temperature kinetic model for the butene isomers based on a validation against low-pressure laminar premixed flames. However this study did not include some reactions essential to the ignition process in the low- to intermediate-temperature range. Most recently, Law and co-workers [15] reported laminar flame speeds and ignition temperatures for non-premixed counter-flow flames at normal and elevated pressures. Their mechanism built on previous studies by Zhang [16] and Cai [17] and included additional rate constants for the reactions of isobutene with $\dot{H}$ and $\ddot{O}$ atoms and $\dot{O}H$, $H\dot{O}_2$ and $\dot{C}H_3$ radicals.

In view of the above considerations, we can see that, there is a lack of experimental data available in the literature for isobutene at low temperatures (600–1000 K) and at high pressures (>10 atm), which are conditions of direct relevance with respect to gasoline, diesel, and HCCI engine technologies.

2. Experimental methods

Table1. Ignition delay time, flame speed data and speciation data for isobutene oxidation used for as validation target in this study.

Reactor	T (K)	P (atm)	ϕ	Dilution	Ref.
Parameter range for isobutene oxidation available in the literature					
Ignition delay time					
Shock tube	1200–1980	2.2–4.6	0.1–4.0	80.8–98.8%	[10]
Speciation					
JSR	790–1250	1.0–10.0	0.2–2.0	>95%	[12]
Flow reactor	1139–1150	1.0	0.42–1.29	>94%	[11]
Flame speed					
Flat flame burner	298	1.0–10.0	0.7–1.8	'air'	[15]
Parameter range for isobutene oxidation available in this study					
Ignition delay time					
Shock tube	940–1500	1.7–50	0.3–2.0	'air'	
RCM	666–996	10–50	0.3–2.0	'air'	
Flame speed					
Flat flame burner	298–398	1.0	0.6–1.9	'air'	
Spherical Flame	298	1.0	0.75–1.5	'air'	

Table 1 compares the experimental conditions investigated as part of this study to those of studies found in the literature. Ignition delay times for isobutene oxidation were measured in four different shock tube facilities and two rapid compression machines (RCMs) shown below. Laminar flame speeds for isobutene were measured at the Université de Lorraine (LRPG). Spherical flame speed measurements were also recorded at Princeton University (PU) and TAMU. All experimental data are provided in the appended Supplementary material.

2.1 NUI Galway (NUIG) high-pressure shock tube

Ignition delay times were measured in the high-pressure shock tube at NUIG described in the recent study by Burke *et al*. [2]. Ignition delay times were recorded for isobutene/'air' mixtures at φ = 0.3, 0.5, 1.0 and 2.0 at pressures of approximately 10, 30 and 50 atm and in the temperature range of approximately 940–1500 K. The ignition delay time was defined as the interval between the rise in pressure due to the arrival of the reflected shock wave at the endwall and the maximum rate of rise of the pressure signal, as shown in Figure 1.
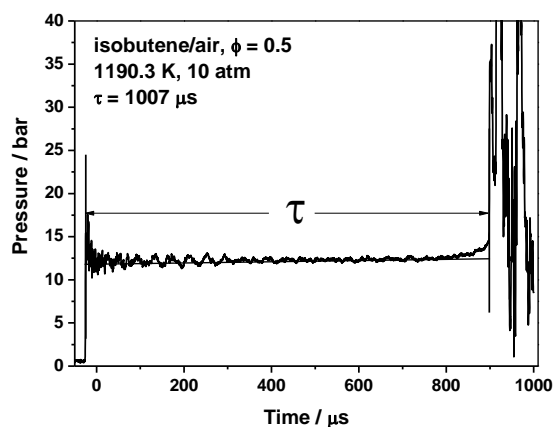

Figure 1. Sample pressure trace from NUI Galway shock tube.

2.2 Texas A&M University (TAMU) shock tube

Details and a schematic of the shock-tube setup are provided in Aul *et al*. [18]. All experimental methods were identical to those used in our recent collaborative study of propene ignition [2]. Ignition delay times for isobutene/O_2/Ar mixtures were measured at φ = 0.5, and 1.0 with isobutene concentration ranges from 0.143% to 2% at pressures of 1.7 and 10 atm and in the temperature range of 1050–1765 K.

In addition to the endwall and sidewall transducers to monitor the test pressure, the chemiluminescence emission from the excited hydroxyl radical (OH*) located on the sidewall was also used to monitor the kinetics of the reaction. To detect possible pre-ignition events that could occur during the tests, Chemiluminescence was also recorded using another photomultiplier but without a filter at the endwall location. Ignition delay time from the three measurements shown in Figure 2(a) and (b) predict very similar results.
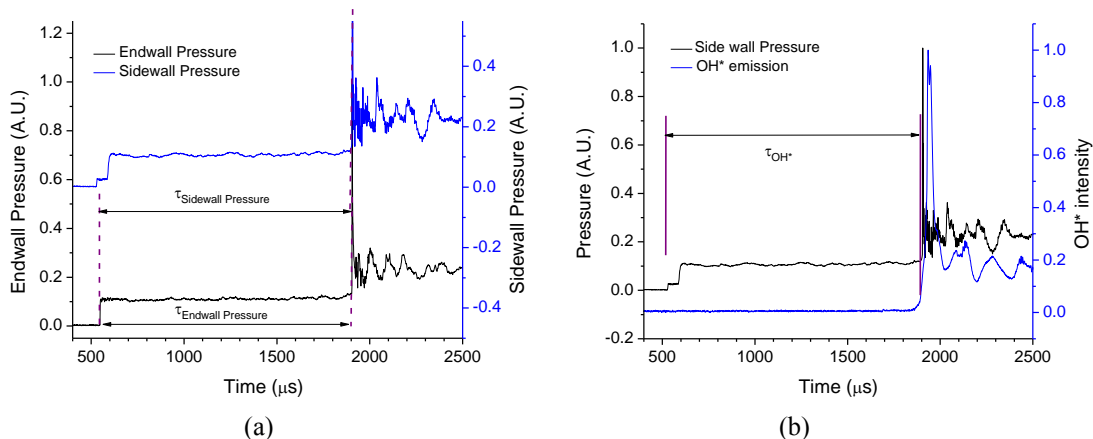
Figure 2. Ignition delay time measurements in the TAMU shock tube at 1222 K, ϕ =1.0, 2% isobutene in Ar, 9.34 atm. (a) Pressure sensors located at both the endwall and sidewall locations. (b) Pressure and OH* emission measurements.

2.3 Rensselaer Polytechnic Institute (RPI) shock tube

Measurements of isobutene ignition delay times were made at RP in the high-pressure shock tube described by Shen and Oehlschlaeger [19]. All experimental methods were identical to those used in our recent collaborative study of propene ignition [2]. For the present experiments with isobutene, which is gaseous at standard conditions, shock tube heating was not necessary. Ignition delay times were measured for isobutene/air mixtures at φ = 0.5, 1.0, and 2.0 at pressures around 10 atm and for isobutene/12% O_2/Ar mixtures for φ = 1.0 and 2.0 at pressures around 10 and 40 atm. Reactant mixtures were made outside the shock tube in a mechanically-stirred mixing vessel. Isobutene was from Aldrich at 99+% purity and O_2, N_2, and Ar were 99.995% pure from Noble Gas. Following reactant mixture preparation and mechanical mixing (4 h), reactant test gases were loaded into the shock tube driven section and ignition delay experiments performed. Ignition delay time determinations were made behind reflected shock waves by measuring the pressure at a side wall location 2 cm from the driven section end wall and hydroxyl radical emission (OH*) viewed through the driven section end wall. The onset of ignition was defined by extrapolating the maximum slope in OH* signal to the baseline and time-zero was defined as the time of shock reflection at the end wall, determined from the measured pressure and incident shock velocity. Figure 3 illustrates an example measurement. The reflected shock conditions were determined using the normal shock relations with input of the measured incident shock velocity, determined via the incident shock passage over a series of five pressure transducers spaced over the last meter of the driven section. The uncertainty in reflected shock temperature and pressure is estimated at approximately ±1% and ±1.5%, respectively, for the conditions considered in this study. The uncertainty in ignition delay time is estimated at ±20%, based on contributions from uncertainty in reflected shock conditions and in determination of ignition delay from measured signals. The measured reflected shock pressure profiles show non-ideal pressure rise of $(dp/dt)(1/p_0)$ = 2–3%/ms at the conditions studied.
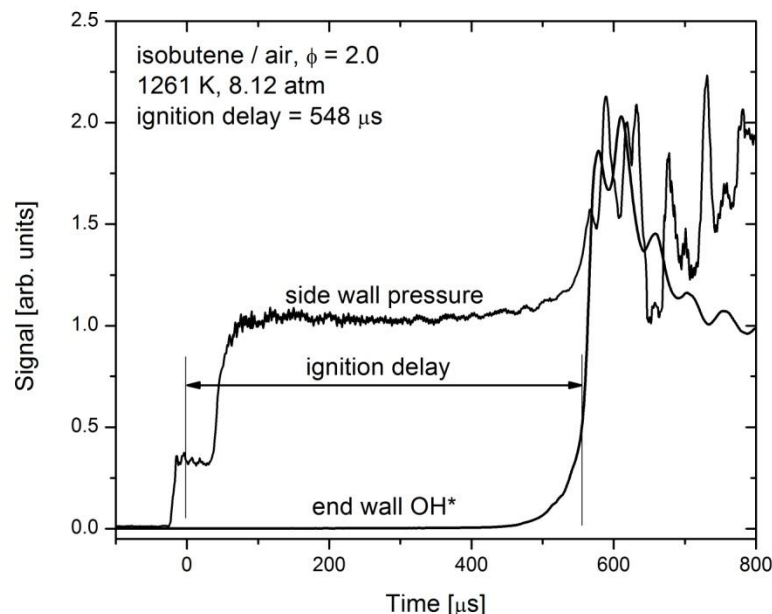
Figure 3. Example isobutene ignition delay time measurement from the Rensselaer facility.

2.4 King Abdullah University of Science and Technology (KAUST) shock tube

Ignition delay times for isobutene/'air' mixtures at φ = 0.5, 1.0 and 2.0 at 40 atm were measured at KAUST in the high pressure shock tube. All experimental methods were identical to those used in our recent collaborative study of propene ignition [2]. The experimental setup is shown in Fig. 7 by Burke *et al* [2]. Ignition delay time is defined as the time from the arrival of the reflected shockwave to the onset of ignition at the sidewall. Three diagnostics, pressure trace and the OH* emission detected at the endwall and the sidewall, are used to determine the onset of ignition. The three methods predict very similar ignition delay times, as illustrated in Figure 4.
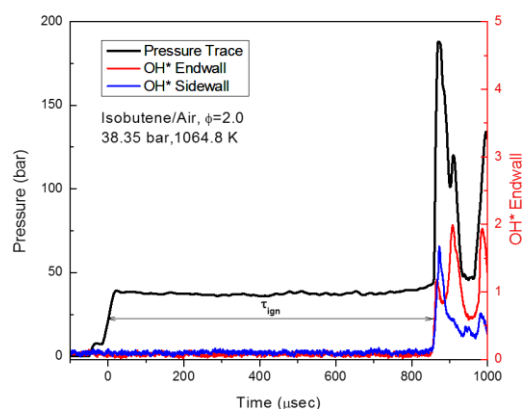
Figure 4. Example of isobutene ignition delay time measurement from the KAUST shock tube.

2.5 NUI Galway rapid compression machine

Ignition delay times for isobutene/'air' mixtures at φ = 0.3, 0.5, 1.0 and 2.0 at pressures of approximately 10, 30 and 50 atm were measured at NUIG in the rapid compression machine and are similar to those described in the recent propene study by Burke et al. [2]. The ignition delay time definition in this work is shown in Figure 5 and is taken from the time of peak pressure at the end of compression to the time of maximum rate of pressure rise due to ignition.
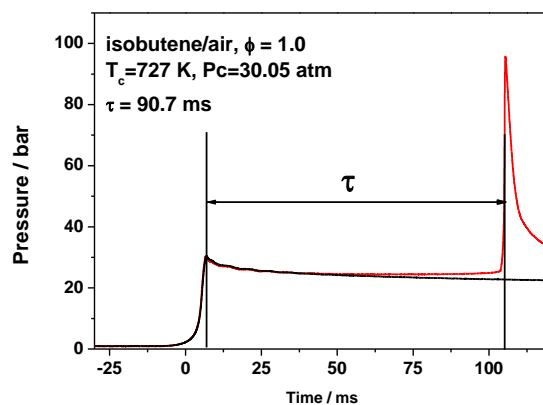
7

Figure 5. Sample pressure traces from NUI Galway RCM. —— Non-reactive profile, —— reactive profile.

2.6 University of Connecticut (UConn) rapid compression machine

The rapid compression machine (RCM) at UConn employs a creviced piston to compress test mixtures to elevated pressures and temperatures. The creviced piston is driven pneumatically and brought to rest by hydraulic pin-groove mechanism towards the end of the compression stroke. While the typical compression times are around 30−45 ms, the majority of pressure/temperature rise occurs in the last 6 ms of compression, as shown in Fig. 1. A trigger from LabVIEW[®] initiates the compression event and starts data acquisition. Dynamic pressure in the reaction cylinder is measured using a thermal-shock resistant Kistler 6125C transducer in conjunction with 501B charge amplifier. Test gas mixtures can be compressed to desired test conditions, compressed pressure (p_c) and compressed temperature (T_C), by independently varying compression ratio, intake pressure (p_0), and intake temperature (T_0). Compression ratios varying between 7 and 17 can be attained by varying stroke length or/and clearance length. Moreover, compressed temperature (T_C) is deduced using the adiabatic core hypothesis.

Reaction cylinder is filled to the desired intake pressure (p_0) with a homogenous fuel/oxidizer mixture prepared in a separate stainless steel mixing chamber of 17.47 L, which is equipped with heaters to preheat a fuel/oxidizer mixture to the desired intake temperature (T_0). In the current study, isobutene (>99%) supplied by Sigma-Aldrich and ultra-high purity (>99.99%) O_2 and N_2 from Airgas are used to prepare homogenous isobutene/'air' mixtures in mixing chamber. The 'air' used in these experiments is a mixture of O_2 and N_2 in the molar ratio of 1:3.76. Fuel/oxidizer mixtures are prepared by filling the mixing chamber with fuel and constituent oxidizer gases to the corresponding partial pressures manometrically. The mixing chamber, intake manifold, and reaction cylinder are heated to the desired preheat temperature for about 4 hours before starting the experiments. Additionally, the mixing chamber is equipped with a magnetic stirrer which aids in preparation of homogeneous mixtures. Further details about the current RCM design and test procedure can be found in Das *et al.* [20].

Figure 6 shows the typical experimental repeatability and the definition of ignition delay used for reporting the present data. Ignition delay is defined as the time difference between the end of compression (EOC) and the maxima of time derivative of the pressure after EOC. A minimum of four consecutive runs are conducted at each condition and the value close to the mean of the measured ignition delays is reported as the representative value. The scatter in ignition delays is less than 10% of the representative value for all the cases investigated. Furthermore, to ensure repeatability, ignition delay data obtained from each fresh mixture is checked with that from an earlier mixture.
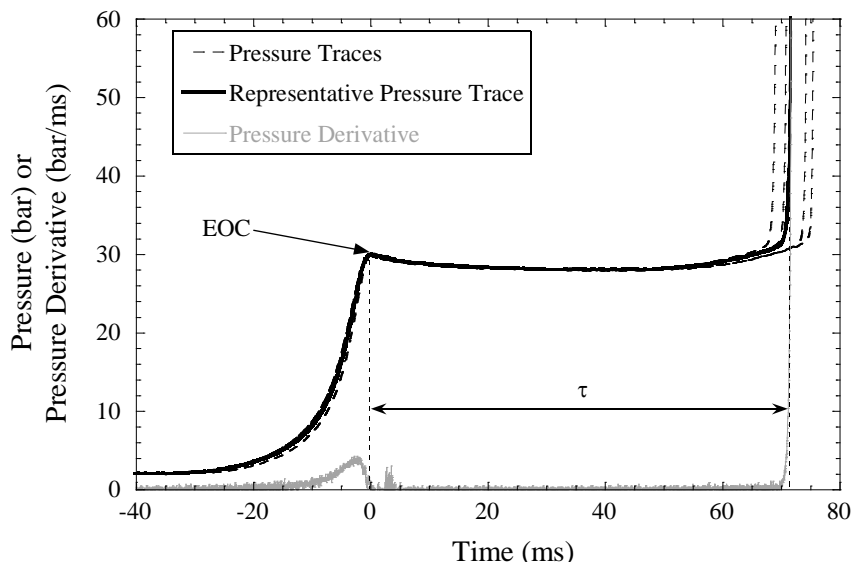
8

Figure 6. Plot showing experimental repeatability and definition of ignition delay at φ = 2.0 in air, p_C = 30 bar, T_C = 686 K, τ = 72 ms.

In order to account for the effect of heat loss to the reactor walls on ignition delay, non-reactive experiments corresponding to each reactive run are taken to infer heat loss characteristics during compression and post compression periods. In these nonreactive experiments, isobutene/N_2 mixtures are prepared by replacing O_2 with N_2 in the corresponding reactive mixtures while maintaining the same fuel concentrations such that a similar specific heat ratio is maintained and similar heat loss conditions exist between the reactive case and the nonreactive case. Pressure traces from nonreactive runs are further used to generate volume time histories in conjunction with the adiabatic core hypothesis. These volume histories are then imposed on auto-ignition simulations for characterizing the heat loss effect during the compression stroke and the post compression event.

2.7 Shock tube simulations

Shock tube simulations were performed as zero-dimensional calculations and begin at the onset of the reflected shock period. The reflected shock pressure (p_5) and temperature (T_5) were used as the initial pressure and temperature, respectively. Constant volume, homogeneous and adiabatic conditions are assumed behind the reflected shock wave and no facility effects were necessarily included. For ignition delay calculations, the simulated ignition delay time is defined to be consistent with the particular diagnostic used in the experiment being simulated. The mechanism presented in this study contains a sub-mechanism for both excited $CH^\star$ and $OH^\star$ which have been adopted from Hall and Petersen [21], and Kathrotia *et al*. [22], respectively.

2.7.1   Brute-force sensitivity

"Brute force" sensitivity analyses were carried out in order to identify the key reactions which control fuel reactivity. The analyses were performed by increasing and decreasing each reaction rate expression by a factor of two and calculating the effect on the predicted ignition delay time.

The sensitivity coefficient is defined as: $S = \frac{\ln(\tau_+/\tau_-)}{\ln(k_+/k_-)} = \frac{\ln(\tau_+/\tau_-)}{\ln(2.0/0.5)}$, where, τ_+ is the ignition delay time calculated with the increased rate coefficient and τ_- is the ignition delay time calculated using the decreased rate coefficient. A positive sensitivity coefficient indicates an inhibiting reaction while a negative sensitivity coefficient indicates a reaction promoting reactivity.

9

2.8 Rapid compression machine simulations

The ignition delay time simulations of the RCM use a volume profile generated from the corresponding nonreactive pressure trace, for which an experiment is performed by replacing oxygen with nitrogen in the fuel/air mixtures. The volume history used for the simulation included the heat loss during the compression stroke by adding an empirically determined additional volume, and the heat loss after the end of compression was accounted for by the "adiabatic core expansion" approach [23-25]. Non-reactive pressure-time traces are taken to correspond to each unique p_c and T_C condition studied. The volume history is then used as an input in the CHEMKIN-PRO [26] input file.

2.9 Flame speeds

Laminar flame speeds for isobutene were measured in three different facilities, which are located at Texas A&M University (TAMU), Princeton University (PU) and Université de Lorraine (LRPG).

2.9.1   Texas A&M flames

Laminar flame speed experiments were conducted in the high-temperature, high-pressure, constant-volume bomb at TAMU. This vessel has an internal diameter of 31.8 cm and an internal length of 28 cm. Optical access is gained through fused-quartz windows located on either end of the vessel, each with a diameter of 12.7 cm. The flame is centrally ignited by two electrodes. This vessel with its relatively large volume allows for the flame to propagate at near constant pressure for the course of the experiment, which ends when the flame reaches the diameter of the 12.7-cm window aperture. Full details on this experimental setup are given in Krejci et al [27].

Mixtures were prepared using the partial pressure method with a 0–1000 Torr pressure transducer. Instrument-grade isobutene and Primary Standard Air were used to conduct all experiments. The initial conditions were 1 atm and 298 K ± 2K. Images were taken using a Z-type Schlieren setup and a high-speed camera (Photron Fastcam SA1.1) at a rate of 6,000 fps. These images were then processed using an internally developed MATLAB-based edge detection program. The burned, un-stretched laminar flame speed was extracted using the appropriate nonlinear method depending on the Markstein length as outlined by Chen [28]. Images that clearly showed either an ignition effect or a wall effect, based on the *dr/dt* versus stretch plot, were neglected. The unburned, un-stretched flame speed was then determined using the density ratio calculated from the equilibrium chemistry.

2.9.2   Princeton University flames

Mass burning rates (the product of flame speed and unburned mixture density) were measured using the spherical flame method in a 10 cm diameter cylindrical chamber with a concentric pressure release chamber and two optical windows with details are shown in [29]. All experimental methods were identical to those used in our recent collaborative study of propene ignition [2]. Mixtures were created from bottled air and isobutene (>99%, Airgas) using the partial pressure method. To reduce compositional uncertainty caused by low fuel partial pressure, lean mixtures were prepared by first creating a rich mixture, allowing the mixture to homogenize for 10 minutes, partially evacuating the chamber, and then diluting with further air to reach the target equivalence ratio and pressure.

2.9.3   CNRS-Université de Lorraine flames

The laminar burning velocities of isobutene oxidation were measured at LRGP using the same atmospheric pressure heat flux burner as that used to study propene flames [2], as well as of components of natural gas [30] and gasoline [31, 32]. The burning velocity of isobutene/air mixtures has been measured under atmospheric pressure at unburned gas temperatures of 298 K, 358 K, and 398

K and for equivalence ratios in the range 0.6–1.9. Isobutene was provided by Air Liquide (purity >99.5%, without any noticeable content of other hydrocarbons). The uncertainty in the laminar burning velocity is the same as we proposed for propene/air mixtures.

2.10 Flame speed simulations

Flame speeds were simulated by the Premix module of CHEMKIN PRO. A high-temperature version which removes all the low temperature chemistry was created to simulate the flame speed to avoid the high computational cost of using the full mechanism. The species removed include the 2-methylallyl radical self-recombination product, alkyl-peroxyl radicals, hydroperoxyl-allyl radicals, ketohydroperoxide species etc. Metcalfe *et al*. [33] carried out extensive tests of flame speed calculations for C0–C2 molecular species using AramcoMech 1.3 and found that the high-temperature mechanism results in the same predictions as the full mechanism with a considerably reduced computational time. Inclusion of the more accurate multicomponent simulations was not necessary as when they were compared to predicted flame speeds using the mixture-averaged option they were within 1 cm s^{-1} of them, but required significantly longer computational times. Thermal diffusive effects were also accounted for and generally resulted in a noticeable reduction in flame speed. The CHEMKIN-PRO was also used to perform the flame speed sensitivity analyses

3. Computational method

Rate constants calculations have been carried out for the following important reactions associated with isobutene oxidation:

- $iC_4H_8 + \dot{O}H \leftrightarrow i\dot{C}_4H_7 + H_2O$
- $iC_4H_8 + \dot{O}H \leftrightarrow i\dot{C}_4H_7\text{-i1} + H_2O$
- $iC_4H_8 + H\dot{O}_2 \leftrightarrow i\dot{C}_4H_7\text{-i1} + H_2O$
- $i\dot{C}_4H_7 \leftrightarrow C_3H_4\text{-a} + \dot{C}H_3$

The M062X method [34] with the 6-311++G(d,p) basis set were used in the geometry optimizations and frequency calculations of all of the species involved in this reaction using Gaussian 09 [35]. The same method was used to determine the potential energy surface scans for the individual hindered rotors associated with reactant and transition state. The electronic single point energies have been calculated at QCISD(T)/cc-pCXZ level of theory (where X = T and Q) which were extrapolated to the complete basis set (CBS) limit [36, 37].

Conventional transition-state theory [38] with an asymmetric Eckart tunneling correction [39] has been used to calculate the high-pressure limit rate constants in this work. The low-frequency torsional conserved modes were treated as hindered rotors using a Pitzer-Gwinn-like approximation [40] to calculate the partition function.

4. Chemical kinetic mechanism development

The current mechanism development is based on the H$_2$/O$_2$ sub-mechanism adopted from the study of Kéromnès et al. [41], the C1–C2 sub-mechanism, AramcoMech 1.3, adopted from the study of Metcalfe and co-workers [33] and the propene/allene/propyne sub-mechanism adopted from the recent publications of Burke et al. [2, 3]. During these developments, the mechanism has been validated against numerous experimental conditions and targets. Key reactions for isobutene oxidation at different temperature and pressure conditions were highlighted by sensitivity analyses for reflected shock ignition delay times, flux analyses and flame speed sensitivity analyses. The isobutene combustion chemistry model developed in *this work* has improved the predictions against a variety of experimental results. The comprehensive kinetic mechanism, thermochemistry and transport files will

be provided as Supplementary material and will also be available to download at http://c3.nuigalway.ie/mechanisms.html.

4.1 Important reaction classes highlighted

Figure 7 highlights the important reactions controlling isobutene fuel oxidation at 10 and 30 atm and at fuel-lean ($\phi = 0.3$) and fuel-rich ($\phi = 2.0$) conditions at intermediate temperatures. The reactions of $iC_4H_8 + \dot{O}H \leftrightarrow i\dot{C}_4H_7 + H_2O$, $i\dot{C}_4H_7 + i\dot{C}_4H_7 \leftrightarrow H15DE25DM$ and $i\dot{C}_4H_7 + \dot{C}H_3 (+M) \leftrightarrow aC_5H_{10}$ $(+M)$ inhibit reactivity for both fuel-lean and fuel-rich conditions at intermediate temperatures. When the pressure increases, the 2-methylallyl ($i\dot{C}_4H_7$) radical self-recombination reaction becomes more favored and inhibits the reactivity more pronouncedly than at lower pressures.

The reactions of $i\dot{C}_4H_7$ with $H\dot{O}_2$ radicals are the most promoting ones at intermediate temperatures in both fuel-lean and fuel-rich mixtures. This is due to the formation of the highly reactive $\dot{O}H$ radicals and methyl-allyloxyl ($iC_4H_7\dot{O}$) radicals; the latter ultimately decompose to produce 2-propenyl ($\dot{C}_3H_5$-t) radicals through different reaction pathways. These $\dot{C}_3H_5$-t radicals react with O_2 to form $CH_3CO\dot{C}H_2$ radicals and $\ddot{O}$ atoms which ultimately promotes reactivity. It is interesting to note that H-atom abstraction from iC_4H_8 by O_2 to form $i\dot{C}_4H_7$ and $H\dot{O}_2$ radicals is the most promoting reaction for fuel-rich mixtures ($\phi = 2.0$). This is because, at fuel-rich conditions, the concentration of the fuel is high and the two products, $i\dot{C}_4H_7$ and $H\dot{O}_2$ radicals, will react further to produce methyl-allyloxy radical ($iC_4H_7\dot{O}$) and the highly reactive $\dot{O}H$ radical. The reaction of $iC_4H_8 + \dot{O}H \leftrightarrow i\dot{C}_4H_7$–i1 $+ H_2O$ promotes reactivity at all conditions studied, as the vinylic isobuten1-yl radical ($i\dot{C}_4H_7$–i1) reacts with molecular oxygen to form $CH_3COCH_3 + H\dot{C}O$ and $iC_3H_5CHO + \dot{O}H$, promoting reactivity. The formation of iC_3H_5CHO mainly through the decomposition of $iC_4H_7\dot{O}$ radicals via the reaction $iC_4H_7\dot{O} \leftrightarrow iC_3H_5CHO + \dot{H}$ is also an important species at intermediate temperatures. With a very weak bond strength ($iC_3H_5CO\cdots H$) of 87.1 kcal mol^{-1}, the aldehydic hydrogen atom is quite easy abstractable to form an $iC_3H_5\dot{C}O$ radical, which decomposes to form CO and a $\dot{C}_3H_5$-t radical which promotes reactivity; that is also the reason why the reaction $iC_3H_5CHO + \dot{O}H \leftrightarrow iC_3H_5\dot{C}O + H_2O$ promotes reactivity.

When the temperature increases to 1250 K, the reaction $iC_4H_8 + O_2 \leftrightarrow i\dot{C}_4H_7 + H\dot{O}_2$ is the most dominant one promoting reactivity at both fuel-lean and fuel-rich conditions over the entire pressure range investigated here, Figure 8. The 2-methylallyl radical self-recombination reaction is not observed to be important at higher temperatures as it readily decomposes.
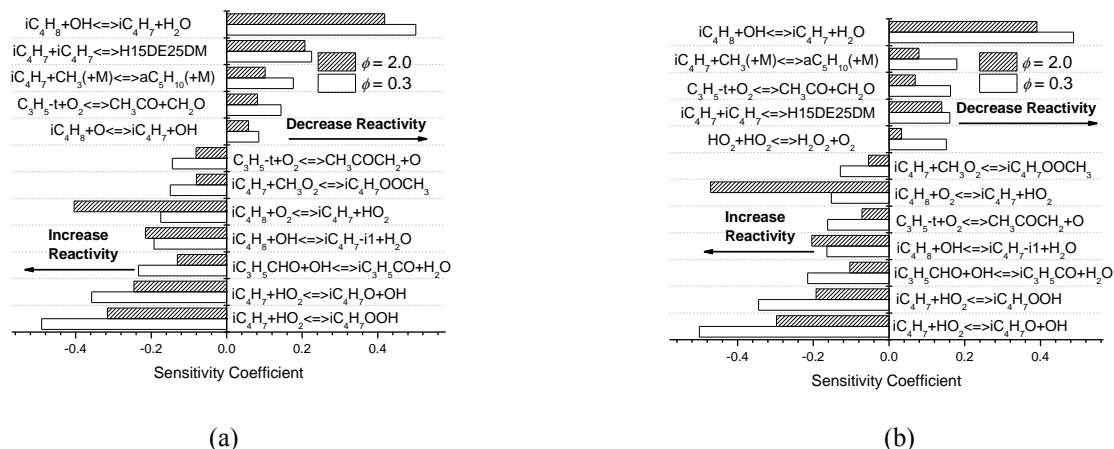

(a)　　　　　　　　　　　　　　　　(b)

Figure 7. "Brute force" sensitivity analyses to ignition delay times performed at (a) $T = 950$ K, $p = 30$ atm, $\phi = 0.3$, and 2.0, (b) $T = 900$ K, $p = 10$ atm, $\phi = 0.3$, and 2.0.
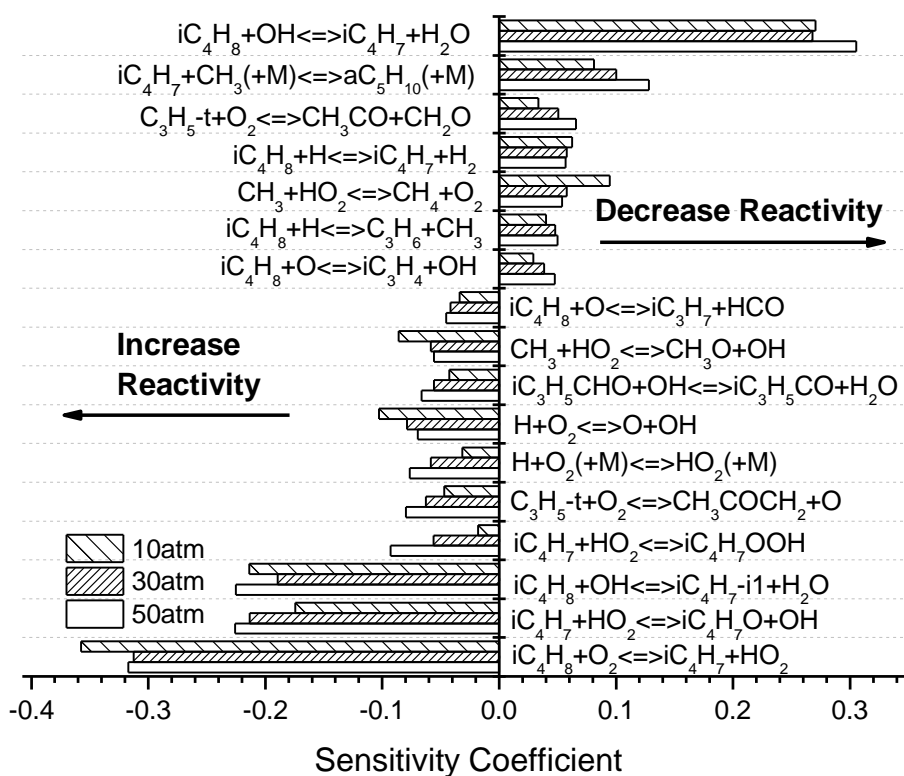
12

Figure 8. "Brute force" Sensitivity analyses to ignition delay times performed at $\phi = 1.0$, fuel/air, $T = 1250$ K and different pressures.

All of the reactions highlighted here will be discussed in detail in the following sections and the detailed reaction pathways are shown in Figure 10. From the bond dissociation energy (BDE) comparison of propene and isobutene shown in Figure 9, we can see that the BDE of the C–C bond in isobutene is 2.0 kcal mol^{-1} lower than that in propene and the allylic C–H bond in isobutene is 0.8 kcal mol^{-1} higher than in propene. Thus, for some of the important reaction rate constants, we use analogous rate constants from propene for isobutene with some reasonable adjustment; for some of the important reaction rate constants we also carried out *ab initio* calculations. Moreover, details of the choice of rate constants are discussed and explained in the following sections.
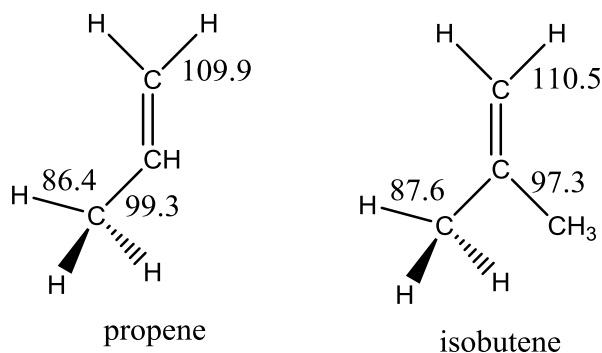
Figure 9. Bond dissociation energy (in kcal/mol) comparison between propene and isobutene obtained at QCISD(T)/CBS//M062x/6-311++G(d,p) at 0 K.
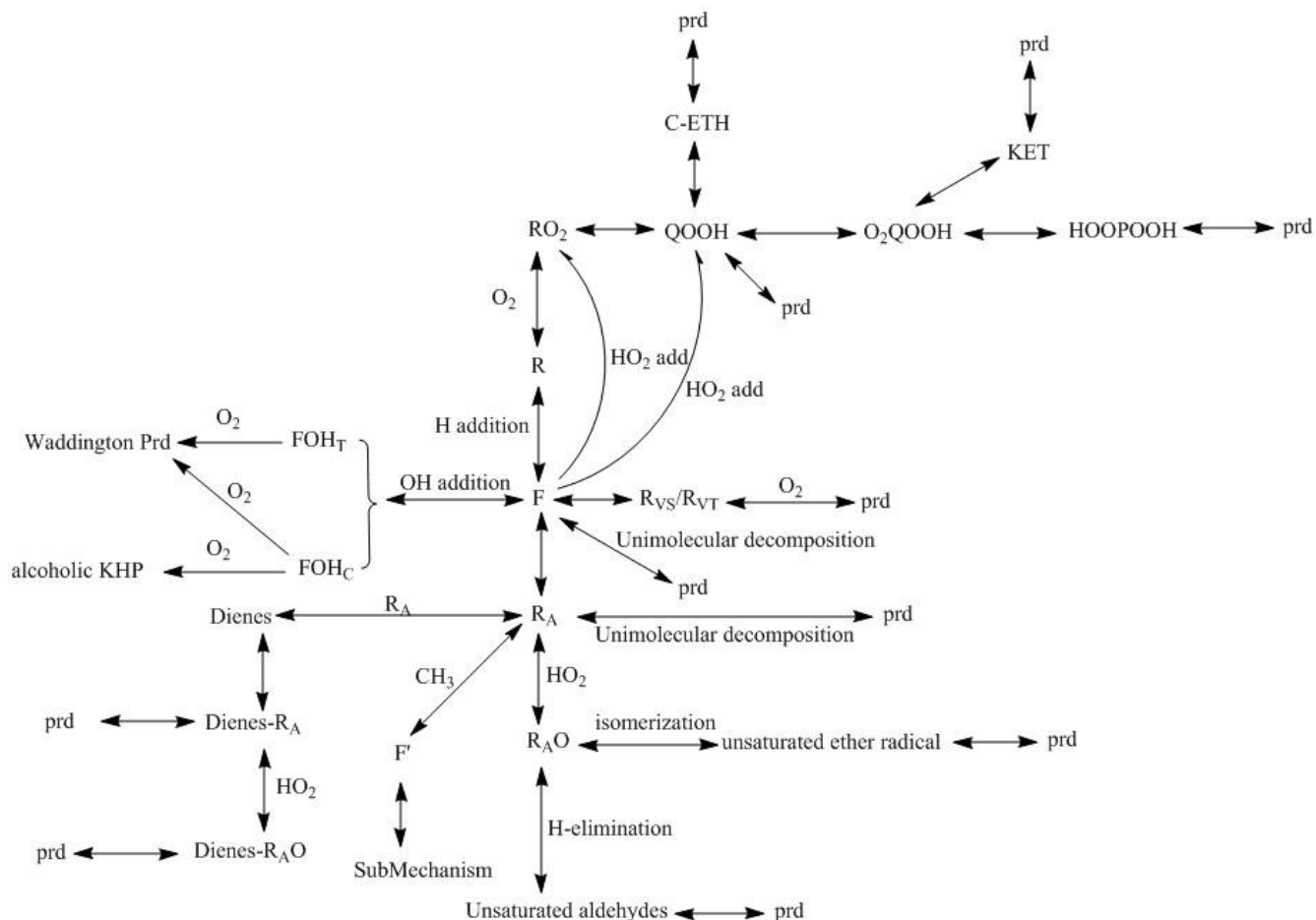
Figure 10. Reaction pathways included in this work for isobutene oxidation. F: fuel; R_A: allylic radical, R_{VS}: vinylic secondary radical; R_{VS}: vinylic tertiary radical; R_AO: methyl-allyloxyl radical; F': 2-methyl-1-butene; alcoholic KHP: alcoholic keto-hydroperoxide; Dienes:2,5-dimethyl-1,5-hexadiene.

4.2 Unimolecular decomposition

Two important reaction channels highlighted here are the allylic C–H bond fission reaction channel which has the lowest bond dissociation energy (forming 2-methylallyl ($i\dot{C}_4H_7$) radical and a $\dot{H}$ atom) and the C–C bond fission reaction channel (forming $\dot{C}_3H_5$-t and $\dot{C}H_3$ radicals):

- $iC_4H_8 \leftrightarrow i\dot{C}_4H_7 + \dot{H}$
- $iC_4H_8 \leftrightarrow \dot{C}_3H_5$-t + $\dot{C}H_3$

Speciation measurements of isobutene pyrolysis in the PU flow reactor are sensitive to isobutene decomposition, Figure 11. The high-pressure limit rate constant has been adopted by analogy with propene [42] with further QRRK calculations to estimate the pressure fall off. However in order to improve agreement with flow reactor speciation measurements from Held $et\ al.$ [43], the rate constants for the formation of allyl radical and atomic hydrogen has been increase by a factor of 2. Figure 11 shows the influence of this adjustment.

14
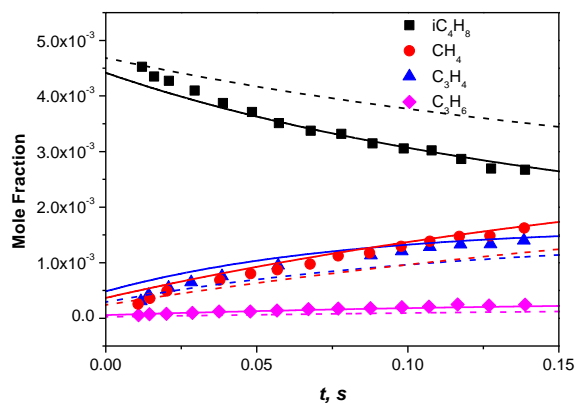
Figure 11. Influence of rate constants for $iC_4H_8 \leftrightarrow i\dot{C}_4H_7 + \dot{H}$ in flow reactor speciation analysis for isobutene pyrolysis. —— *This study*, - - - analogy of propene [42].

4.3 Fuel-radical reactions

H-atom abstraction reactions by various radicals from isobutene have been included in *this work*. There are two different types of hydrogen atom in isobutene that can be abstracted: one from the methyl site forming the resonantly stabilized $i\dot{C}_4H_7$ radical and the other from the terminal carbon to form a vinylic radical ($i\dot{C}_4H_7$-i1). As shown in Figure 9, the bond dissociation energy comparison between those two types of C–H bonds tells us the formation of the 2-methylallyl radical is dominant because it is about 22.9 kcal mol^{-1} weaker than the vinylic one.

4.3.1 $iC_4H_8 + \dot{O}H \leftrightarrow Products$

For the reaction of $\dot{O}H$ radicals with isobutene, both abstraction and addition pathways are included in the current kinetic mechanism.

4.3.1.1 H-Abstraction by $\dot{O}H$ radicals

As shown in Figure 7 and Figure 24, predicted ignition delay times are highly sensitive to the H-atom abstraction reaction by $\dot{O}H$ radicals from isobutene forming 2-methylallyl ($i\dot{C}_4H_7$) radicals in a very large range of temperatures and pressures. This reaction inhibits reactivity throughout the entire temperature range of the ignition delay time measurements, because it consumes a highly reactive $\dot{O}H$ radical and forms a resonantly stabilized and thus relatively unreactive $i\dot{C}_4H_7$ radical. The $i\dot{C}_4H_7$ radicals undergo radical–radical self-recombination or can react with methyl radicals via chain terminating reactions which inhibit reactivity. Rate constants for the reaction of isobutene with $\dot{O}H$ radicals has been reported by Sun *et al.* [44] at the CCSD(T)/6-311++G(d,p)//BH&HLYP/6-311G(d,p) level of theory. As this reaction dominates reactivity over the entire temperature range, we have also calculated the rate constants in this work at a higher level of theory (QCISD(T)/CBS//M062X/6-311++G(d,p)) to obtain more accurate electronic energies and rate constants. Figure 12 shows that the two calculation results are at worst 40% different from one another with different curvature.
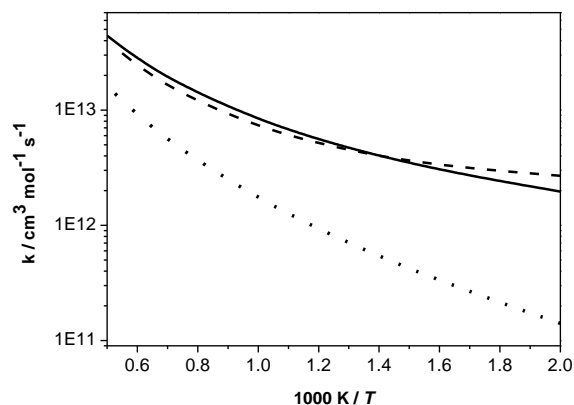
Figure 12. Rate constants comparison of $iC_4H_8 + \dot{O}H$. 2-methylallyl radical formation: —— *This study (ab-initio)*, ˉˉˉˉ Sun *et al.* [44]; vinylic isobuten1-yl radical formation: ······ *This study (ab-initio)*.

4.3.1.2 $\dot{O}H$ addition to iC_4H_8

$\dot{O}H$ radical addition to iC_4H_8 is important at temperatures lower than 850 K and the analogous rate constants from propene plus $\dot{O}H$ radical as calculated by Zador *et al*. [45] were used in this work.

- $iC_4H_8 + \dot{O}H \leftrightarrow i\dot{C}_4H_8OH\text{-it}$
- $iC_4H_8 + \dot{O}H \leftrightarrow i\dot{C}_4H_8OH\text{-ti}$
- $iC_4H_8 + \dot{O}H \leftrightarrow iC_4H_7OH + \dot{H}$
- $iC_4H_8 + \dot{O}H \leftrightarrow sC_3H_5OH + \dot{C}H_3$
- $iC_4H_8 + \dot{O}H \leftrightarrow iC_3H_5OH + \dot{C}H_3$
- $iC_4H_8 + \dot{O}H \leftrightarrow sC_4H_7OH\text{-i} + \dot{H}$
- $iC_4H_8 + \dot{O}H \leftrightarrow CH_3COCH_3 + \dot{C}H_3$
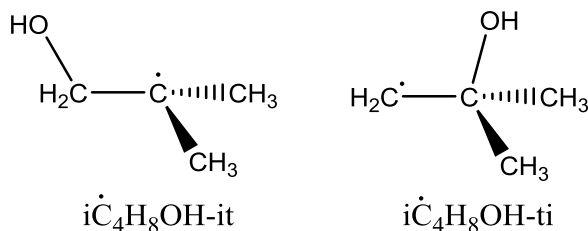
Figure 13. Structures of the two species formed by $\dot{O}H$ radical addition to iC_4H_8.

The competition between the formation of $i\dot{C}_4H_8OH\text{-it}$ and $i\dot{C}_4H_8OH\text{-ti}$ radicals, Figure 13, plays a significant role in dictating the predicted reactivity in the low temperature range. Rather than taking the branching ratio of these two channels as being 50:50, we altered it to be 75:25 and keep the total rate constants the same as that for $\dot{O}H$ added to propene. The influence to the ignition delay times in the low temperature range can be seen in Figure 14; this reaction does not influence the high temperature ignition delay time. From the flux analysis shown in Figure 25 we observe that at 730 K and 30 atm, $\dot{O}H$ radical addition reaction consumes 21.7% of the fuel, with 17.3% of the fuel forming $i\dot{C}_4H_8OH\text{-it}$ radicals through terminal addition and 4.4% forming $i\dot{C}_4H_8OH\text{-ti}$ radicals through addition to the central carbon atom. When the temperature increases to 850 K, only 7.9% of iC_4H_8 is consumed through terminal addition and central addition no longer contributes at all. As the temperature increases further to 950 K, $\dot{O}H$ radical addition reactions do not contribute to fuel consumption.
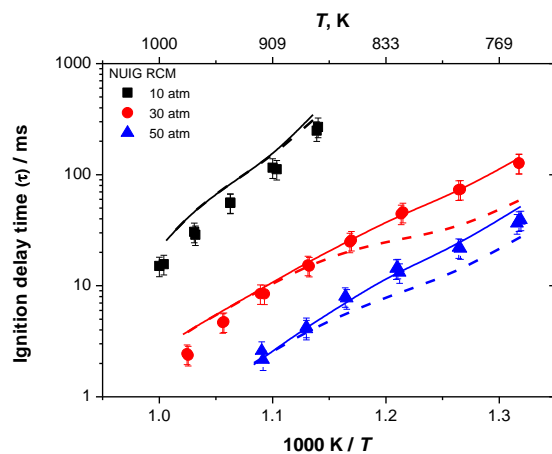
Figure 14. Branching ratio effects from the $\dot{O}H$ terminal and central addition to iC_4H_8 to ignition delay times at $\phi=0.5$, fuel in air, $p = 10$, 30 and 50 atm. Terminal vs. central: solid line (75:25); dashed line (50:50).

4.3.1.3 Addition of $i\dot{C}_4H_8OH$-it and $i\dot{C}_4H_8OH$-ti radicals to O_2

Sun *et al.* [46] calculated the rate constants of $i\dot{C}_4H_8OH$-it and $i\dot{C}_4H_8OH$-ti radical addition to O_2 and their subsequent decomposition reactions. They used canonical transition state theory to calculate the elementary rate constants and quantum Rice-Ramsperger-Kassel (QRRK) theory to calculate pressure- and temperature-dependent rate constants. As shown in Figure 25, the formation of CH_3COCH_3, CH_2O and $\dot{O}H$ radical is the dominant product set resulting from $i\dot{C}_4H_8OH$-it radical addition to O_2.

For the addition of $i\dot{C}_4H_8OH$-ti radicals to O_2, the competition between the two reaction channels dictates the reactivity of the system, the formation of CH_3COCH_3, CH_2O and $\dot{O}H$ radical (the typical Waddington mechanism) inhibits reactivity, while the channel forming a ketohydroperoxide species promotes reactivity.
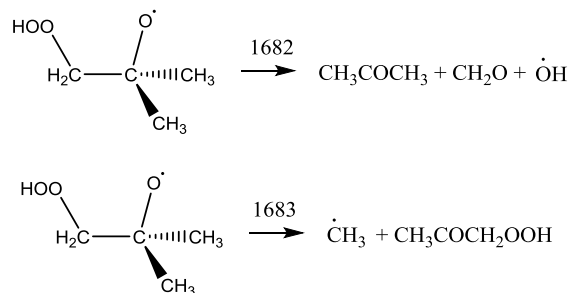
When we compared the analogous high-pressure limit rate constants for these two channels from Villano et al. [47] are quite different from the rate constants obtained by Sun et al. [46]. We have used rate constants for reactions 1682 and 1683 estimated by analogy with those calculated by Villano et al. [47] for $\dot{C}_3CCOOH\Leftrightarrow C_2C=C+CH_2O+\dot{O}H$ and $\dot{C}_2CCOOH\Leftrightarrow C=CCOOH+\dot{C}H_3$ respectively; we found the reactivity has been captured much better especially in the lower temperatures shown in Figure 15. After this adjustment, the flux analysis in Figure 25 shows that the improvement in the lower temperature reactivity is from the chaining branching reactions from the second O_2 addition, even with 4.4% initial formation of $i\dot{C}_4H_8OH$-ti radical, this influence is quite large Figure 16. Our current treatment captures the low temperature reactivity of isobutene oxidation quite well; while further fundamental research studies to provide accurate pressure and temperature dependence rate constants for the first and second addition to molecular oxygen reactions are needed to give a better understanding of the low temperature chemistry of alkene fuel oxidation.

(a) ϕ=0.3, fuel in air

(b) ϕ=0.5, fuel in air

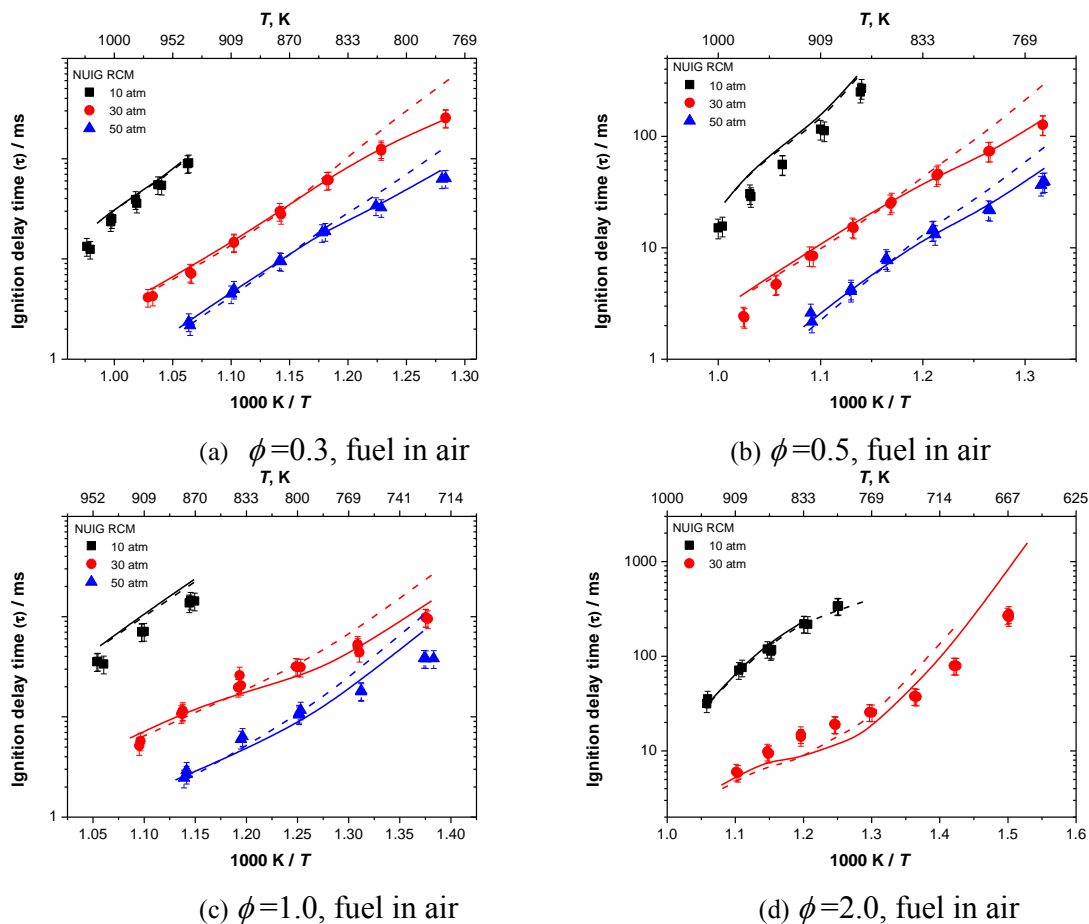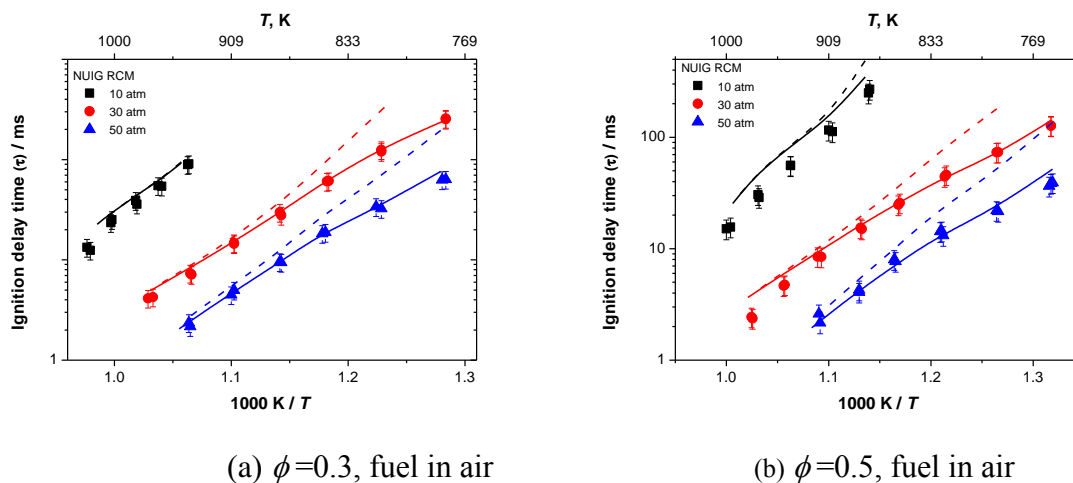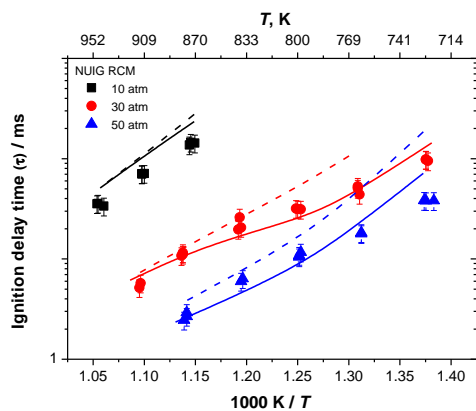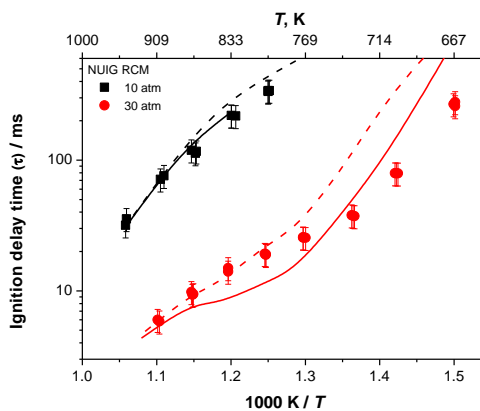(c) ϕ=1.0, fuel in air

(d) ϕ=2.0, fuel in air

Figure 15. Influence of replacing rate constants for reactions 1682 and 1683 from Sun et al. [46] (dashed line) to Villano et al. [47] (solid line) to ignition delay time.

The second addition to molecular oxygen has also been included and its influence to the ignition delay times at lower temperatures is shown in Figure 16. The rate constants for the reaction channels are taken by analogy to rate constants from Miyoshi [48] for the entrance channel of the second (hydroperoxyl-alkyl) radical addition to molecular oxygen and Goldsmith [49] for the following isomerization and decomposition reaction channels.

(a) ϕ=0.3, fuel in air

(b) ϕ=0.5, fuel in air

(c) ϕ=1.0, fuel in air   (d) ϕ=2.0, fuel in air

Figure 16. Model predictions by including (solid line) and excluding (dashed line) the second addition to molecular oxygen reaction class on ignition delay times prediction.

4.3.2 $iC_4H_8 + \dot{H} \leftrightarrow Products$

Flux analyses have identified the reaction between isobutene and hydrogen atom is important, Figure 25. At low and intermediate temperatures (< 950 K), hydrogen atom addition to isobutene inhibits reactivity as the $t\dot{C}_4H_9$ radicals formed mostly decompose to iC_4H_8 and a $\dot{H}$ atom. Sensitivity analyses (Figure 8) shows that the formation of propene and a $\dot{C}H_3$ radical inhibits reactivity at higher temperatures as it forms an unreactive $\dot{C}H_3$ radical from a very reactive hydrogen atom, and this reaction also competes with the main chain branching reaction promoting reactivity, $\dot{H} + O_2 \leftrightarrow \ddot{O} + \dot{O}H$.

Previously [2, 3], the estimated high-pressure limit rate constants for these reaction channels from Curran [50] were used in the mechanism. In this study, we used analogous rate constants for $\dot{H}$ atom addition to, and abstraction from, propene calculated by Miller and Klippenstein [51] at a high level of theory to describe the potential energy surface. Conventional transition state theory was used to calculate the abstraction reactions rate constants; RRKM theory was used to calculate micro-canonical, J-resolved rate constants for the dissociation processes, and master-equation methods to determine phenomenological rate constants for all of the non-abstraction reactions.

4.3.3   iC4H8 + ĊH3 ↔ Products

Similar to H-atom abstraction by $\dot{O}H$ radicals described above, methyl radicals can abstract two different types of H-atom from isobutene to form 2-methylallyl radicals plus methane and/or isobuten1-yl radicals plus methane, respectively. However, only the channel producing 2-methylallyl radicals and methane was found to occur. This reaction is predicted to be an important source of methane detected in the JSR. We have adopted the rate constants provided by Yasunaga et al. [9] in our mechanism.

4.3.4 $iC_4H_8 + H\dot{O}_2$ ↔ Products

Both the H-abstraction reaction channels by $H\dot{O}_2$ radical and the $H\dot{O}_2$ radical addition reaction channels have been taken into consideration.

H-abstraction reaction by $H\dot{O}_2$

- $iC_4H_8 + H\dot{O}_2 \leftrightarrow i\dot{C}_4H_7 + H_2O_2$
- $iC_4H_8 + H\dot{O}_2 \leftrightarrow i\dot{C}_4H_7\text{-i1} + H_2O_2$

The rate constant for the H-abstraction reactions of isobutene by hydroperoxyl radical forming 2-methylallyl radical ($i\dot{C}_4H_7$) is adopted from the theoretical study of Zádor et al. [52]. The rate constant for the other H-abstraction channel forming the vinylic isobuten1-yl ($i\dot{C}_4H_7$-i1) radical was calculated in this work.

4.3.4.1 $H\dot{O}_2$ addition to iC_4H_8
- $iC_4H_8 + H\dot{O}_2 \leftrightarrow i C_4H_9\dot{O}_2{}^a$
- $iC_4H_8 + H\dot{O}_2 \leftrightarrow i\dot{C}_4H_8O_2H\text{-t}^b$
- $iC_4H_8 + H\dot{O}_2 \leftrightarrow tC_4H_9\dot{O}_2{}^c$
- $iC_4H_8 + H\dot{O}_2 \leftrightarrow t\dot{C}_4H_8O_2H\text{-i}^c$
- $iC_4H_8 + H\dot{O}_2 \leftrightarrow iC_4H_8O + \dot{O}H^c$
- $t\dot{C}_4H_8O_2H\text{-I} \leftrightarrow iC_4H_8O + \dot{O}H^c$

[a]rate constants from Villano et al. [53] [b]rate constants from Villano et al. [54] [c]rate constants from Zador [52]

The rate constants for the addition reactions of hydroperoxyl radicals to isobutene have been investigated by different groups [52-54]. Zador et al. calculated the rate constants for $H\dot{O}_2$ radical addition to the central unsaturated carbon atom in isobutene to form a hydroperoxy-alkyl radical and its following reaction to form a cyclic ether and an hydroxyl radical. The QCISD(T)/cc-pV∞Z//B3LYP/6-311++G(d,p) level of theory was used to obtain the electronic energy barrier heights, based on which the multi-well master equations were solved to calculate the pressure and temperature dependence of the rate constants. Dean and co-workers did a systematic investigation of alkylperoxyl radical decompositions to alkenes and hydroperoxyl radicals [53], and $H\dot{O}_2$ + olefin addition channels [54] using electronic structure calculations performed at the CBS-QB3 level of theory. The rate constants for the dissociation reactions were obtained from calculated equilibrium constants and a literature review of experimental rate constants for the reverse association reactions. In *this work*, we use rate constants from Villano et al. [53, 54] for the first two reaction channels and for the last four reaction channels rate constants from Zador et al. [52] have been adopted.

iC$_4$H$_8$ + O$_2$ ↔ Products
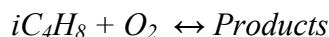
H-atom abstraction by molecular oxygen from isobutene forming iĊ$_4$H$_7$ + HȮ$_2$ radicals was found to be sensitive over the entire temperature range, inhibiting reactivity at lower temperatures and promoting reactivity at higher temperatures.

Several research groups have investigated the reaction between iC$_4$H$_8$ and molecular oxygen. Ingham *et al*. [55] have studied the rate constants in the temperature range 673–793 K. Chen and Bozzelli [56] used canonical transition state theory to calculate the rate constants in the temperature range 300–2000 K. Interestingly, there is a large uncertainty between these two results with a factor of two to five difference in the overlapping temperature range (650–800 K) studied. Goldsmith *et al*. theoretically investigated the reaction of propene with molecular oxygen as part of their study of the reactions between allyl and hydroperoxyl radicals [57]. In order to directly compare this rate constants, they were written in the opposite direction using the CHEMRev software [58]. Yasunaga *et al*. [9] constructed the rate constants for this study to explain product distributions. In *this work,* the rate constants provided by Yasunaga et al. were adopted but were increased by 40–80% over the temperature range. Comparisons of the rate constants are shown in Figure 17.
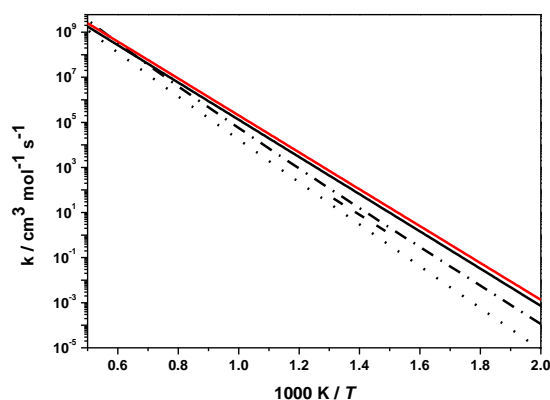
Figure 17. Rate constants comparison of iC$_4$H$_8$ + O$_2$. ——*This study*, —— Yasunaga *et al*. [9], - - - Ingham *et al*. [55], ·····Chen and Bozzelli [56], − ·− Goldsmith *et al*. for propene [57].
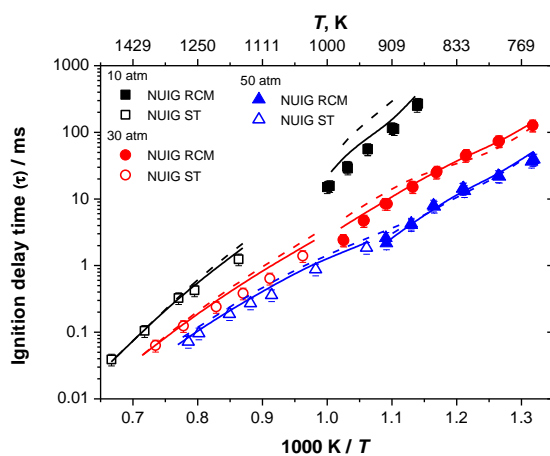
Figure 18. Influence of rate constants for iC$_4$H$_8$ + O$_2$ ↔ iĊ$_4$H$_7$ + HȮ$_2$ to ignition delay times at $\phi = 0.3$, fuel in air, $p = 10$, 30 and 50 atm. Solid line: this study, dashed line: analogy to propene [3].

iC₄H₈ + Ö ↔ Products

Hydrogen atom abstraction by atomic oxygen did not show significant sensitivity in this work. Rate constants for these reactions are adopted from the ones used by analogy for propene [59]. Oxygen atom can also add to isobutene to produce the following products:

- $iC_4H_8 + \ddot{O} \leftrightarrow i\dot{C}_3H_7 + H\dot{C}O$
- $iC_4H_8 + \ddot{O} \leftrightarrow \dot{C}H_2CO + \dot{C}H_3 + \dot{C}H_3$
- $iC_4H_8 + \ddot{O} \leftrightarrow iC_3H_6CO + \dot{H} + \dot{H}$

As shown above, oxygen atom addition reactions form two or more radicals through the three reaction pathways; thus these are chain branching reactions. This reaction class has not been studied previously either experimentally or theoretically. Further experimental or theoretical investigation of this reaction class under combustion conditions will be helpful in improving the accuracy of the model.

4.4 iĊ₄H₇ ↔ Products
- $i\dot{C}_4H_7 \leftrightarrow C_3H_4\text{-a} + \dot{C}H_3$

The decomposition of iĊ₄H₇ radicals will be competitive with its recombination reactions with other radicals such as ĊH₃, HȮ₂, iĊ₄H₇, etc. in the intermediate temperature range. The rate constant for this reaction has been calculated in this work as discussed in Section 3.

4.5 iĊ₄H₇+ R ↔ Products

4.5.1   iĊ₄H₇+ ĊH₃ ↔ aC₅H₁₀

The recombination reaction of 2-methylallyl and methyl radicals to form 2-methyl-1-butene is an important reaction pathway which inhibits reactivity at intermediate and higher temperatures, Figure 7, Figure 8 and Figure 26. The current mechanism predicts that this reaction produces nearly all of the 2-methyl-1-butene detected in the JSR experiments. Our recommended rate constant is taken from Tsang [59] by analogy with allyl and methyl radical recombination.

4.5.2   iĊ₄H₇+ HȮ₂ ↔ products

The reactions of 2-methylallyl and hydroperoxyl radicals are observed to be very important across a range of conditions, especially at low- to intermediate-temperatures, Figure 7 and Figure 25. A rate of production analysis shows that at approximately 730 K, 30 atm, and ϕ =1.0, the reaction of 2-methylallyl radical with hydroperoxyl radical consumes approximately 47.1% of all 2-methylallyl radicals, Figure 25. Pressure dependent rate constants for the bi-molecular reactions of allyl radical with hydroperoxyl radical have been extensively studied by Goldsmith *et al*. [49]; analogous rate constants have been used to describe the reaction between 2-methylallyl radical and hydroperoxyl radical with the following important reaction channels:

- $i\dot{C}_4H_7 + H\dot{O}_2 \leftrightarrow iC_4H_7OOH$
- $i\dot{C}_4H_7 + H\dot{O}_2 \leftrightarrow iC_4H_7\dot{O} + \dot{O}H$
- $iC_4H_7OOH \leftrightarrow iC_4H_7\dot{O} + \dot{O}H$

iC₄H₇O ↔ Products

- $iC_4H_7\dot{O} \leftrightarrow \dot{C}_3H_5\text{-t} + CH_2O$
- $iC_4H_7\dot{O} \leftrightarrow iC_3H_5CHO + \dot{H}$
- $iC_4H_7\dot{O} \leftrightarrow iC_3H_5O\dot{C}H_2$
- $iC_4H_7\dot{O} \leftrightarrow iC_3H_6CHO$

- $iC_4H_7\dot{O} \leftrightarrow C_3H_6 + HC\dot{O}$
- $iC_3H_5CHO \leftrightarrow iC_3H_5\dot{C}O + \dot{H}$
- $iC_3H_5\dot{C}O \leftrightarrow \dot{C}_3H_5\text{-t} + CO$

Methyl-allyloxyl radicals can undergo both decomposition and isomerization reactions to produce different type of products. 2-propenyl radical and formaldehyde, methacrolein and atomic hydrogen, and propene and formyl radicals can be formed through its decomposition reaction. Rate constants for these reactions were taken from the study of Goldsmith *et al.* [57] for propene by analogy. H-atom abstraction from methacrolein (iC_3H_5CHO) to form $iC_3H_5\dot{C}O$ radical and H_2O promotes reactivity at intermediate temperatures (Figure 7, Figure 8, andFigure 24). The rate constant for this reaction channel is taken from the ab initio calculations of Mendes et al. [60]. H-atom abstractions from metharolein by $H\dot{O}_2$ and $\dot{C}H_3$ radicals and $\dot{H}$ atoms have also been included from calculations by Mendes et al. [60].

4.5.3 $i\dot{C}_4H_7/ i\dot{C}_4H_7\text{-}i1 + O_2 \leftrightarrow Products$
- $i\dot{C}_4H_7\text{-}i1 + O_2 \leftrightarrow CH_3COCH_3 + HC\dot{O}$
- $i\dot{C}_4H_7\text{-}i1 + O_2 \leftrightarrow t\dot{C}_3H_6CHO + \ddot{O}$
- $i\dot{C}_4H_7\text{-}i1 + O_2 \leftrightarrow iC_3H_5CHO + \dot{O}H$

Chen and Bozzelli [56] have theoretically studied the reaction mechanism of 2-methylallyl radical. Unlike saturated alkanes in which the fuel molecule radical $\dot{R}$ reacts with O_2 to form an $R\dot{O}_2$ radical with a heat release of ~35 kcal mol^{-1}, for the unsaturated alkenes the analogous reaction process only produces ~20 kcal mol^{-1} of heat, or specifically 21.5 kcal mol^{-1} for $i\dot{C}_4H_7 + O_2 \leftrightarrow iC_4H_7\dot{O}_2$ in this work. The well of the $iC_4H_7\dot{O}_2$ radical formed is shallow and thus back dissociation to $i\dot{C}_4H_7 + O_2$ is favored over the higher barrier isomerization reaction processes. Thus, the reactions of $i\dot{C}_4H_7$ radicals with molecular oxygen are not found to be particularly sensitive in this study. Rate constants for reactions and thermodynamics data for species involved in the $i\dot{C}_4H_7 + O_2$ reactions have been adopted from the study by Chen and Bozzelli [56]. To the best of our knowledge, there are no previous studies of the reaction of isobuten1-yl radical with molecular oxygen; rate constants for this reaction have been adopted by analogy with propene [3].

4.6 2,5-dimethyl,1-5-hexadiene
- $i\dot{C}_4H_7 + i\dot{C}_4H_7 \leftrightarrow H15De25DM$
- $i\dot{C}_4H_7 + i\dot{C}_4H_7 \leftrightarrow C_3H_4\text{-a} + aC_5H_{10}$

2-methylallyl radicals react via chain terminating self-recombination reaction to form 2,5-dimethyl,1-5-hexadiene significantly inhibits reactivity at low- and intermediate-temperatures. The self-recombination of 2-methylallyl radicals can also result in the formation of allene and 2-methyl-1-butene. However, this reaction channel can be neglected as the rate constants is about two orders of magnitude lower than the 2-methylallyl radical self-recombination rate constants and does not contribute to fuel reactivity. Rate constants for this reaction are taken from Tranter and co-workers [61] for the allyl radical self-recombination and have been divided by a factor of 2.3 to match the low temperature ignition delay time measurements, Figure 19. If the $i\dot{C}_4H_7$ radical self-recombination reaction were removed from the system, the reactivity would increase significantly in the lower temperature range as shown in Figure 20.
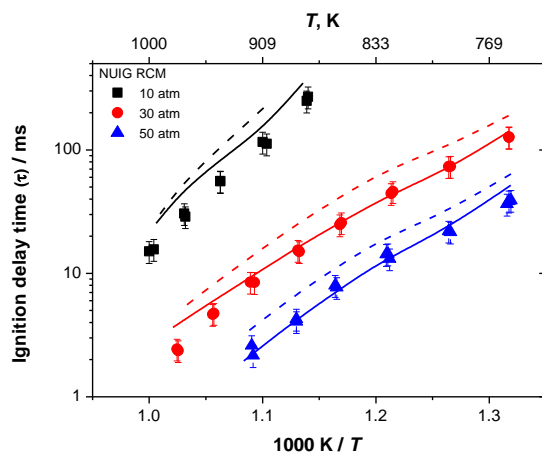
Figure 19. Influence of rate constants for i$\dot{C}_4H_7$ + i$\dot{C}_4H_7$ on ignition delay times at $\phi = 0.5$ in air, $p = 10$, 30 and 50 atm. Solid line: this study, dashed line: same as allyl–allyl from Fridlyand *et al.* [61].
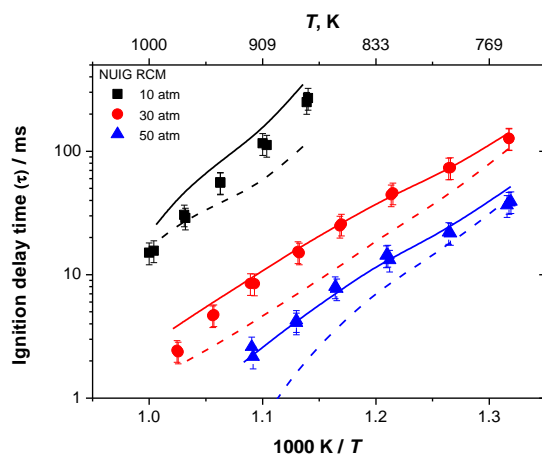

Figure 20. Influence of rate constants for i$\dot{C}_4H_7$ + i$\dot{C}_4H_7$ to ignition delay times at $\phi = 0.5$ in 'air', $p = 10$, 30 and 50 atm. Solid line: this study; dashed line: excluding recombination channel.

4.7 2,5-dimethyl,1-5-hexadiene sub-mechanism
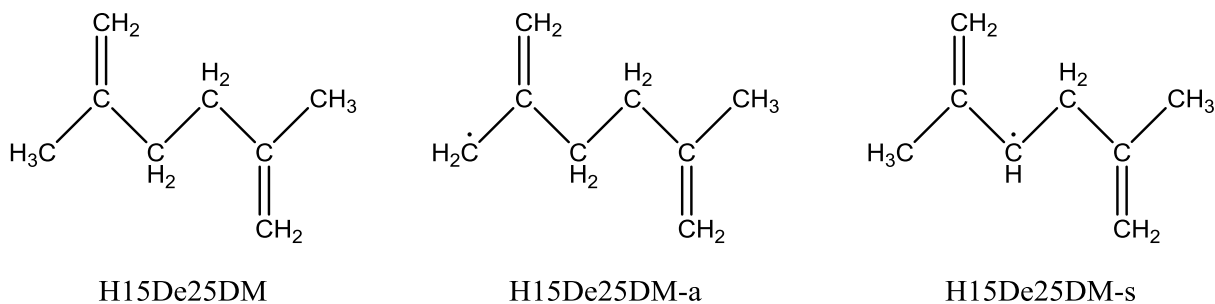
Figure 21. Geometry of 2,5-dimethyl,1-5-hexadiene and the important radicals formed.

As shown in Figure 21, there are two different types of hydrogen atom that can be abstracted in the symmetric structure of 2,5-dimethyl,1-5-hexidene to form the allyl-type radical (H15De25DM-a) and secondary allylic-type radical (H15De25DM-s). H-atom abstraction from 2,5-dimethyl,1-5-hexidene by $\dot{O}H$, $H\dot{O}_2$ and $\dot{C}H_3$ radicals, $\ddot{O}$ and $\dot{H}$ atoms, and O_2 have been taken into consideration in the mechanism. The radicals formed can react with $H\dot{O}_2$ radicals at this low- and intermediate-temperature

range; they can also decompose directly via β-scission. Estimated rate constants are used for their reaction with $H\dot{O}_2$ radical based on analogy with normal alkanes. For the latter two β-scission reactions in the following equation array rate constants were estimated by analogy with propene + CH_2O and acetaldehyde + allyl as recommended by Curran [50].

- H15De25DM-a + $H\dot{O}_2$ ↔ H15De25DM-aO + $\dot{O}H$
- H15De25DM-s + $H\dot{O}_2$ ↔ H15De25DM-sO + $\dot{O}H$
- H15De2M-t + CH_2O ↔ H15De25DM-aO
- iC_3H_5CHO + $i\dot{C}_4H_7$ ↔ H15De25DM-sO

5. Model validations

The current chemical kinetic mechanism is validated against the ignition delay time and flame speed measurements carried out in this work and also the speciation results from a jet-stirred reactor and flow reactor in the literature.

5.1 Ignition delay time validations

Ignition delay times measured from all of our collaborators (four shock tubes and two rapid compression machines) are presented here, together with the predictions of the current mechanism. The current mechanism has captured the experimental results quite well.

A comprehensive comparison between different experimental facilities for both shock tubes and RCMs has been carried out in our previous work in developing the propene mechanism [2] and found that the experimental results of ignition delay time is within 20% between different facilities.

RCMs used in this work are designed differently and each will have different heat loss, therefore different ignition delay times will be provided for the same mixture. In our previous work on propene oxidation ignition delay time measurement [2], we found that the NUIG RCM exhibits more heat loss than the UConn facility. When simulating the ignition delay times from RCM measurements, we adopted the volume history for every experiment as input to account for the specific heat loss for each facility which allows each RCM to be simulated appropriately.

Figure 22 (a)–(d) shows the effect of pressure on ignition delay times measured in shock tubes and RCMs for fuel/'air' mixtures at ϕ = 0.3, 0.5, 1.0, and 2.0. The experimental results show that when pressure increases the ignition delay times decrease at all equivalence ratios. That is because when the pressure increases, the concentrations of reactants also increase so the overall reactivity will increases. The current mechanism predicts the influence of pressure on ignition delay times over a wide range of temperature and equivalence ratios accurately. Sensitivity analyses (Figure 7, Figure 8, and Figure 24) together with flux analyses (Figure 25 and Figure 26) were carried out at different temperatures and pressures to determine the reactivity controlling reactions at those conditions.
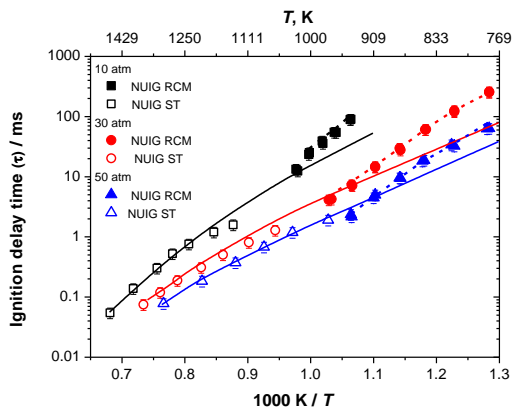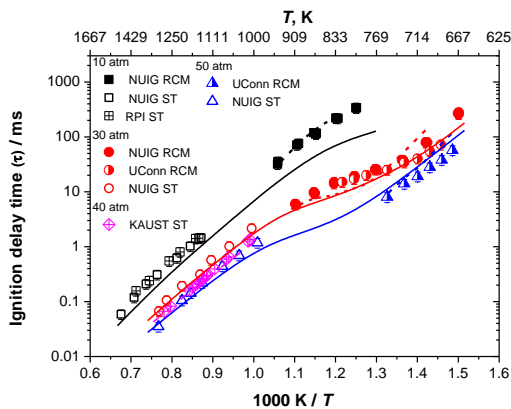
(a) $\phi = 0.3$, fuel/'air', $p = 10$, 30 and 50 atm.
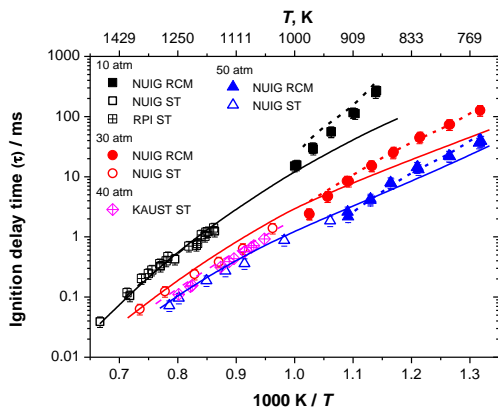
(b) $\phi = 0.5$, fuel/'air', $p = 10$, 30 and 50 atm.
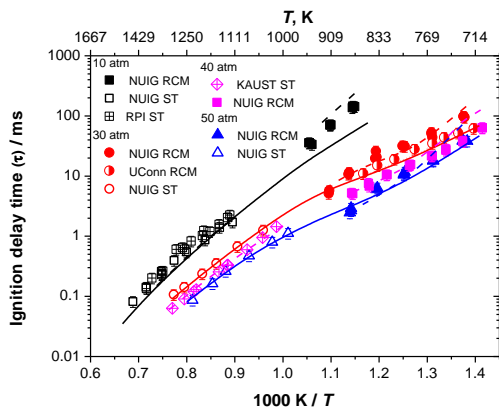
(c) $\phi = 1.0$, fuel/'air', $p = 10$, 30 and 50 atm.

(d) $\phi = 2.0$, fuel/'air', $p = 10$, 30 and 50 atm.

Figure 22. Influence of pressure on isobutene IDTs from shock tube and RCMs for fuel/'air' mixtures. Symbols: experimental data; solid lines: constant volume simulation, dashed lines: facilities effect

Figure 23 (a)–(f) shows a comparison between the ignition delay time measurements from TAMU and RPI against the current mechanism validation. The model captures most of these fuel-lean conditions except at $\phi = 1.0$, fuel in Ar, $p = 1.7$ atm and $\phi = 2.0$, fuel in Ar, $p = 10$ and 40 atm conditions, where the model predicts ignition times that are a little faster than the experimental results.
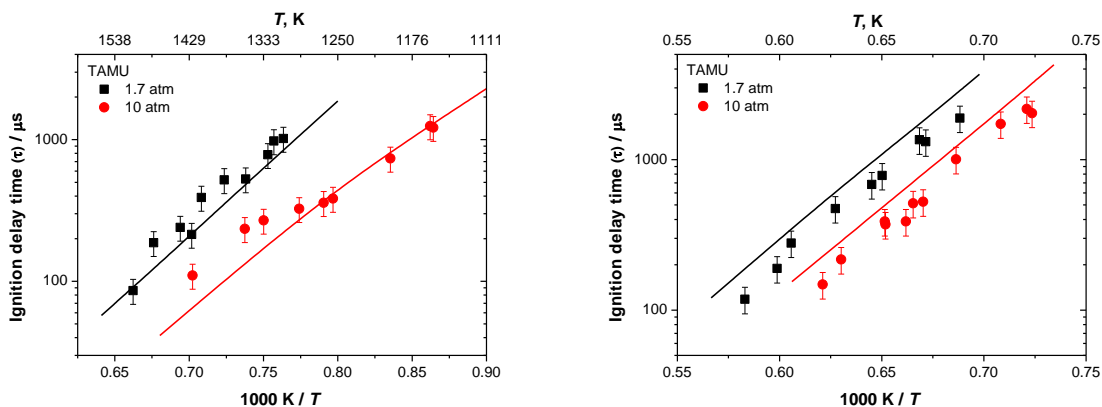
(a) $\phi = 0.5$, fuel/Ar, 1.72% iC_4H_8, $p = 1.7$ and 10 atm. (b) $\phi = 1.0$, fuel/Ar, 0.143% iC_4H_8, $p = 1.1$ and 10 atm.
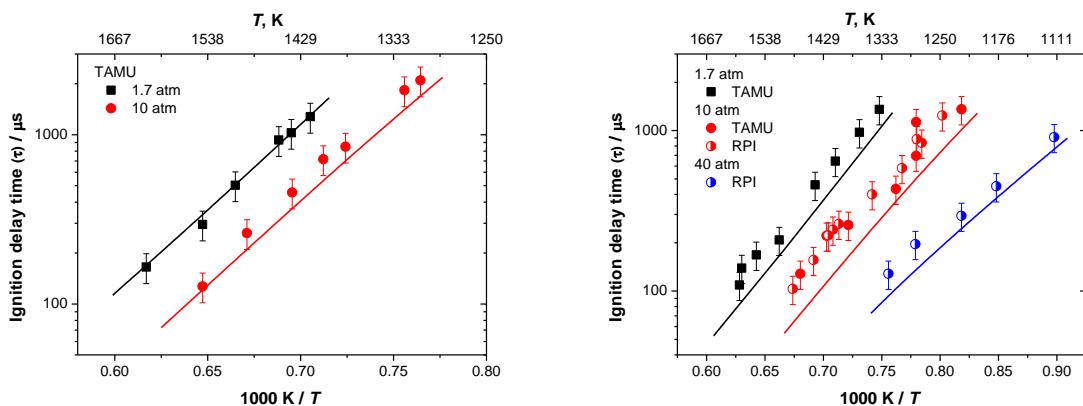
(c) $\phi = 1.0$, fuel/Ar, 0.667% iC_4H_8, $p = 1.7$ and 10 atm. (d) $\phi = 1.0$, fuel/Ar, 2% iC_4H_8.
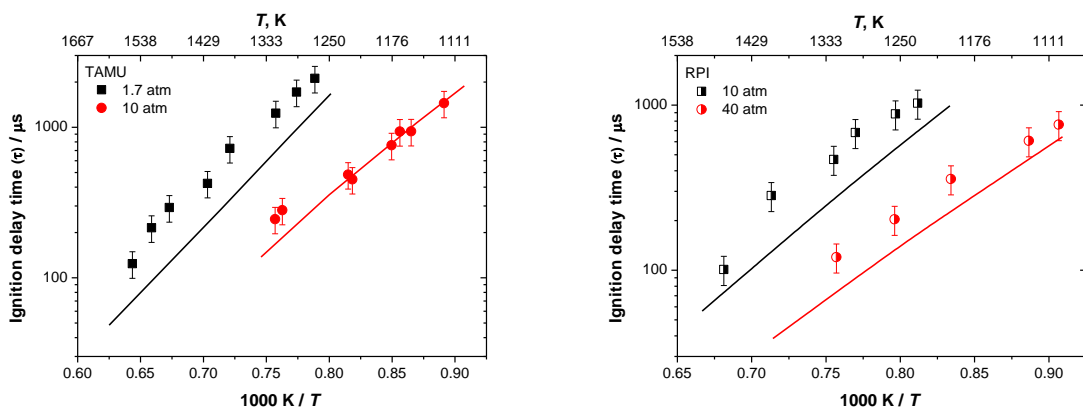
(e) $\phi = 1.0$, fuel/Ar, 3.38% iC_4H_8, $p = 1.7$ and 10 atm. (f) $\phi = 2.0$, fuel/Ar, 4% iC_4H_8, $p = 10$ and 40 atm.

Figure 23. Influence of pressure on isobutene IDTs from TAMU and RPI shock tube measurements for fuel/O_2/Ar mixtures. Symbols: experimental data; solid lines: constant volume simulation.

5.2 Sensitivity and flux analyses

In order to provide an overview of the isobutene combustion pathways that control reactivity, we performed a series of sensitivity analyses at $T = 730$ K, 850 K, 950 K and 1250 K at $\phi = 1.0$ and $p = 30$ atm, Figure 24. Flux analyses at exactly the same conditions have also been carried out, Figure 25 andFigure 26. It is obvious that the $iC_4H_8 + \dot{O}H \leftrightarrow i\dot{C}_4H_7 + H_2O$ reaction inhibits reactivity at all temperatures studied here and its flux increases as the temperature increases.

27

At 730 K, the addition of $\dot{O}H$ radicals to the central carbon atom in iC_4H_8 forming $i\dot{C}_4H_8OH$-ti radicals pronouncedly promotes reactivity. The flux analysis presented in Figure 25 shows that, even though this channel accounts for only 4.4% of the total flux, the subsequent chain branching reactions generating the radical pool ultimately promotes reactivity. Even though the $i\dot{C}_4H_7 + i\dot{C}_4H_7 \leftrightarrow$ H15DE25DM reaction inhibits reactivity, it only contributes 6.5% of the total flux. The addition of $\dot{H}$-atoms to the terminal carbon atom in iC_4H_8 forming $t\dot{C}_4H_9$ radicals consumes 18.6% of the fuel. Thereafter, $t\dot{C}_4H_9$ radicals add to molecular oxygen and largely reforms iC_4H_8 and an $H\dot{O}_2$ radical. It is interesting to find that the reaction of $iC_4H_8 + O_2 \leftrightarrow i\dot{C}_4H_7 + H\dot{O}_2$ inhibits reactivity at 730 K, because the reaction proceeds in the reverse direction, consuming $i\dot{C}_4H_7$ and $H\dot{O}_2$ radicals to form $iC_4H_8 + O_2$ hence preventing chain branching by recombination of methylallyl radicals with $H\dot{O}_2$ radicals, Figure 25. At temperatures above 900 K, this reaction proceeds in the forward direction, promoting reactivity.

At temperatures above 850 K fuel consumption by $\dot{O}H$ radical addition decreases with the overall flux of $\dot{O}H$ radical addition to the terminal carbon dropping to 7.9%. The reaction of $i\dot{C}_4H_7 + i\dot{C}_4H_7 \leftrightarrow$ H15DE25DM becomes important in inhibiting reactivity as it consumes 20.7% of the $i\dot{C}_4H_7$ radicals. This reaction becomes more important at 950 K at which temperature it consumes 39.4% of the $i\dot{C}_4H_7$ radicals. In addition, the radical recombination reaction of $i\dot{C}_4H_7 + \dot{C}H_3 (+M) \leftrightarrow aC_5H_{10} (+M)$ becomes important in inhibiting reactivity, accounting for 7.9% of fuel consumption at 950 K.

At 1250 K, the reaction $iC_4H_8 + O_2 \leftrightarrow i\dot{C}_4H_7 + H\dot{O}_2$ is the most one promoting reactivity in the system. The reaction $i\dot{C}_4H_7 + \dot{C}H_3 (+M) \leftrightarrow aC_5H_{10} (+M)$ which consume 24.6% of the $i\dot{C}_4H_7$ radicals, inhibits reactivity. 26.7% of the $i\dot{C}_4H_7$ radicals formed decompose directly to generate allene and a methyl radical. Interestingly, the self-recombination reaction of $i\dot{C}_4H_7$ to produce H15DE25DM becomes less important at 1250 K, with only 5.6% of $i\dot{C}_4H_7$ radicals consumed by this pathway compared to 39.4% at 950 K. The decreasing dominance of this reaction at high temperatures implies that this reaction pathway will have a minimal effect on ignition delays at high temperatures (Figure 20) and also on laminar flame speed simulations. Thus, this justifies the decision not to include H15DE25DM chemistry for laminar flame speed simulations.
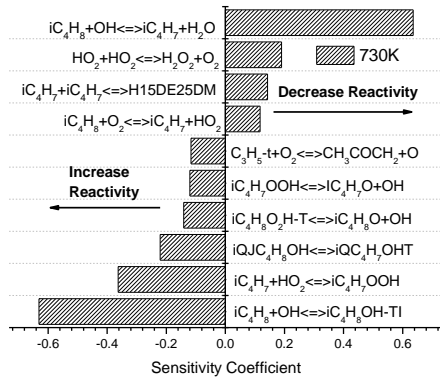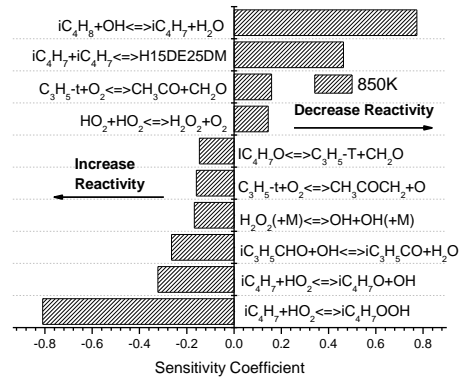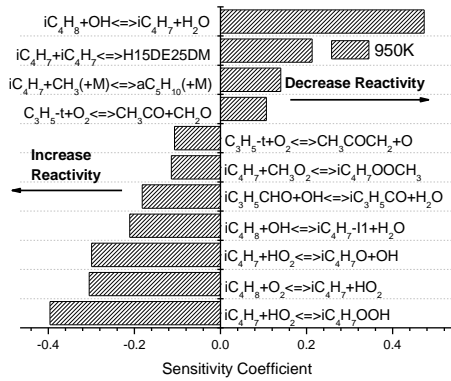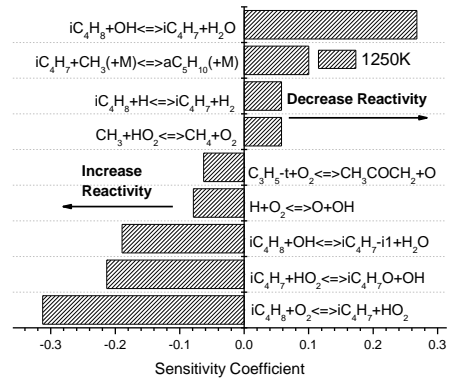
Figure 24. Sensitivity analyses to ignition delay times performed at $\phi = 1.0$, fuel/air, 30 atm, $T = 730$ K, 850 K, 950 K, and 1250 K.
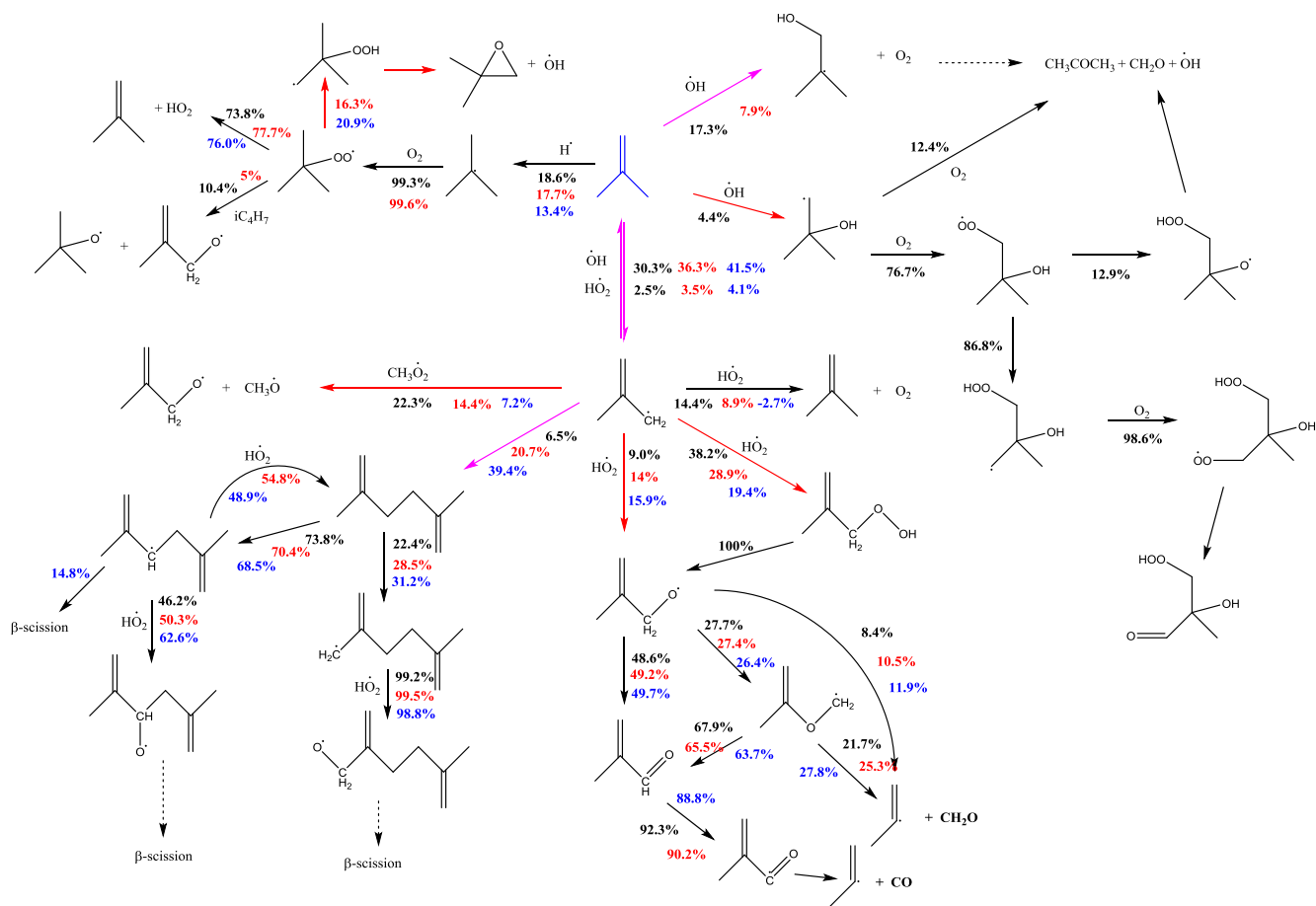
Figure 25. Flux analysis for the oxidation of ϕ =1.0, fuel/air mixture at 730 K (black), 850 K (red) and 950 K (blue) at 20% fuel consumption (red arrows: promote the reactivity; pink ones: inhibit reactivity).
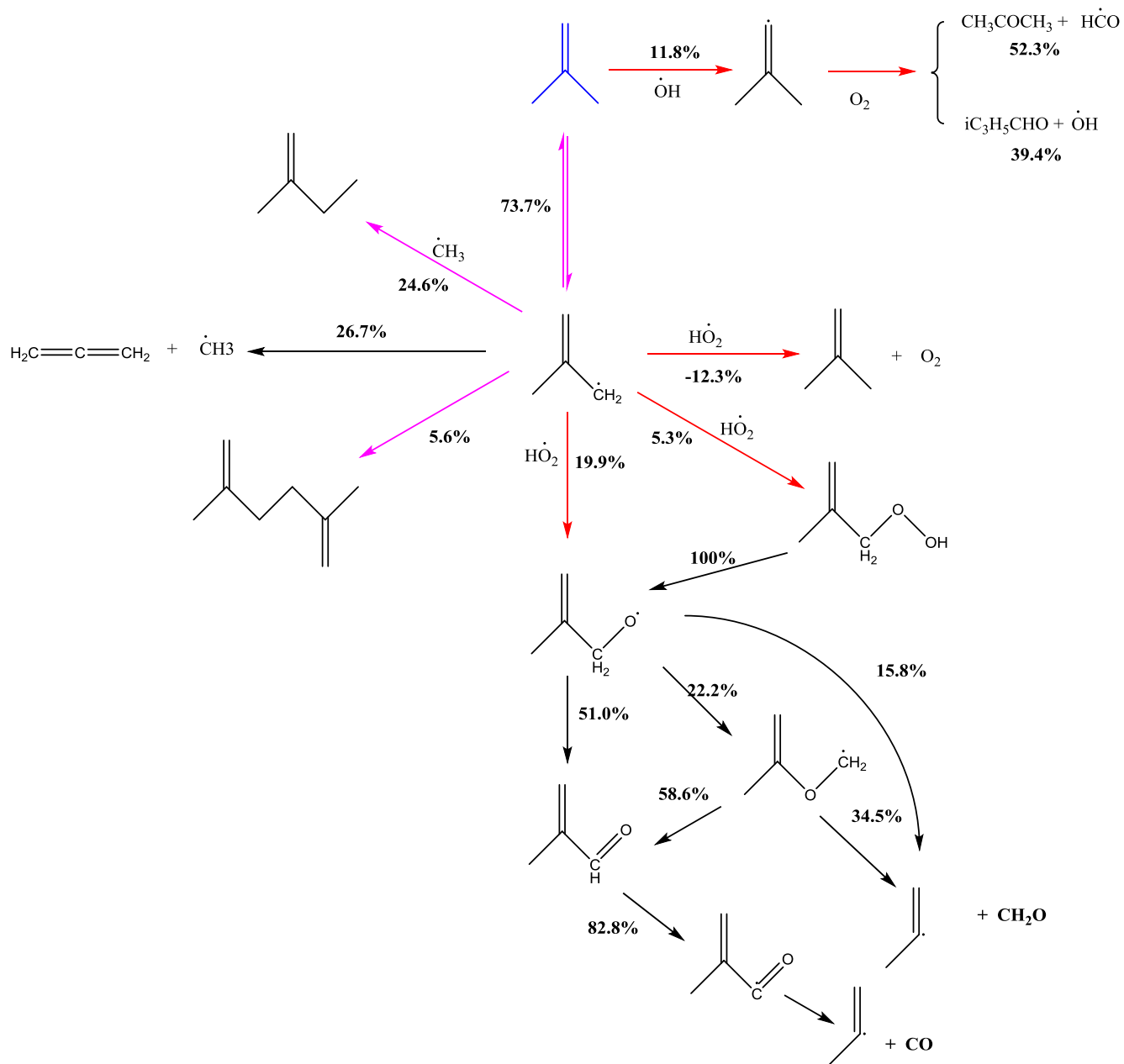
Figure 26. Flux analysis for the oxidation of $\phi =1.0$, fuel/air mixture at 1250 K at 20% fuel consumption. (red arrows: promote the reactivity; pink ones: inhibit reactivity).

5.3 Laminar flame speed results

Figure 27 compares the predicted laminar burning velocities against those measured experimentally for isobutene in air at 1 atm pressure obtained from three different experimental facilities, LRPG, TAMU, and PU. Both the experiments and the simulation show that the temperature increase does not alter the location of the peak flame speed, which expectedly occurs at $\Phi \approx 1.1$. When compared to the experiments performed in the present study, the maximum values are under-predicted by around 5 cm/s, but the locations of these maxima are well predicted. Flame speed sensitivity analyses has been carried out at $\phi = 0.8$, Figure 27 (b). Many of the important reactions highlighted here are from the H_2/CO sub-mechanism. Competition between the chain branching reaction of $\dot{H} + O_2 \leftrightarrow \ddot{O} + \dot{O}H$ and chain propagation reaction of $\dot{H} + O_2 (+M) \leftrightarrow H\dot{O}_2 (+M)$ largely determines the flame

speed predictions. Competition between production of $H\dot{O}_2$ and $\dot{H}$ from formyl radical is also sensitive. The reaction of carbon monoxide with hydroxyl radical is also highlighted here. The highlighted isobutene reactions include $iC_4H_8 + \dot{O}H \leftrightarrow iC_4H_7 + H_2O$, and $iC_4H_8 + \dot{O}H \leftrightarrow iC_4H_7–i1 + H_2O$, but their sensitivity coefficients are minor in comparison to the others discussed, and hence altering the kinetics of these reactions has limited influence on the predicted flame speed.
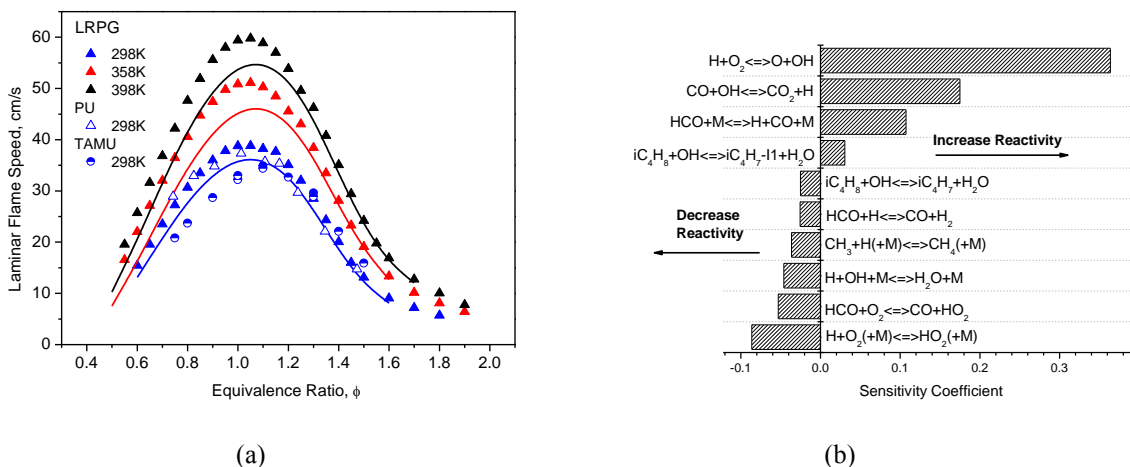

(a)

(b)

Figure 27. (a) Laminar flame speed for iC_4H_8 in air at $p = 1$ atm. Symbols: experimental data, lines: current mechanism. (b) Flame speed sensitivity analysis at $\phi = 0.8$, $T = 298$ K.

5.4 Speciation results

5.4.1 Jet-stirred reactor results

Dagaut et al. [12] have measured the concentration profiles of stable species during the oxidation of isobutene in a jet-stirred reactor at equivalence ratios in the range 0.2–2.0, over a temperature range of 800–1240 K, and in the pressure range 1–10 atm. Overall there is good agreement between the current mechanism and the experimental measurements,
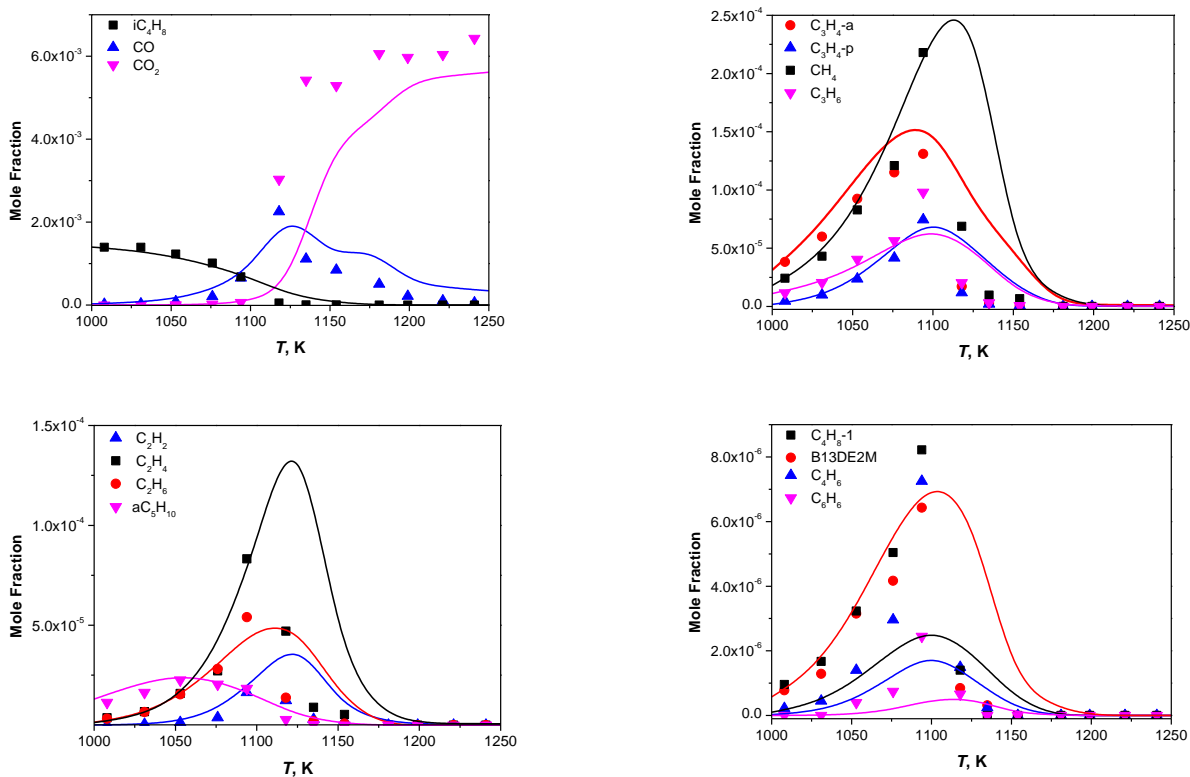
Figure 28–Figure 34. As we discussed above, the H15DE25DM formed through the 2-methylallyl radical self-recombination reaction is a very important intermediate species which was not reported in the JSR experimental results here. Methacrolein (iC_3H_5CHO) which formed through the decomposition of the important methyl-allyoxyl radical is also an important intermediate which is also not reported in the JSR experiments. Future speciation experiments especially for these species measurements will be helpful in the prediction of the model.
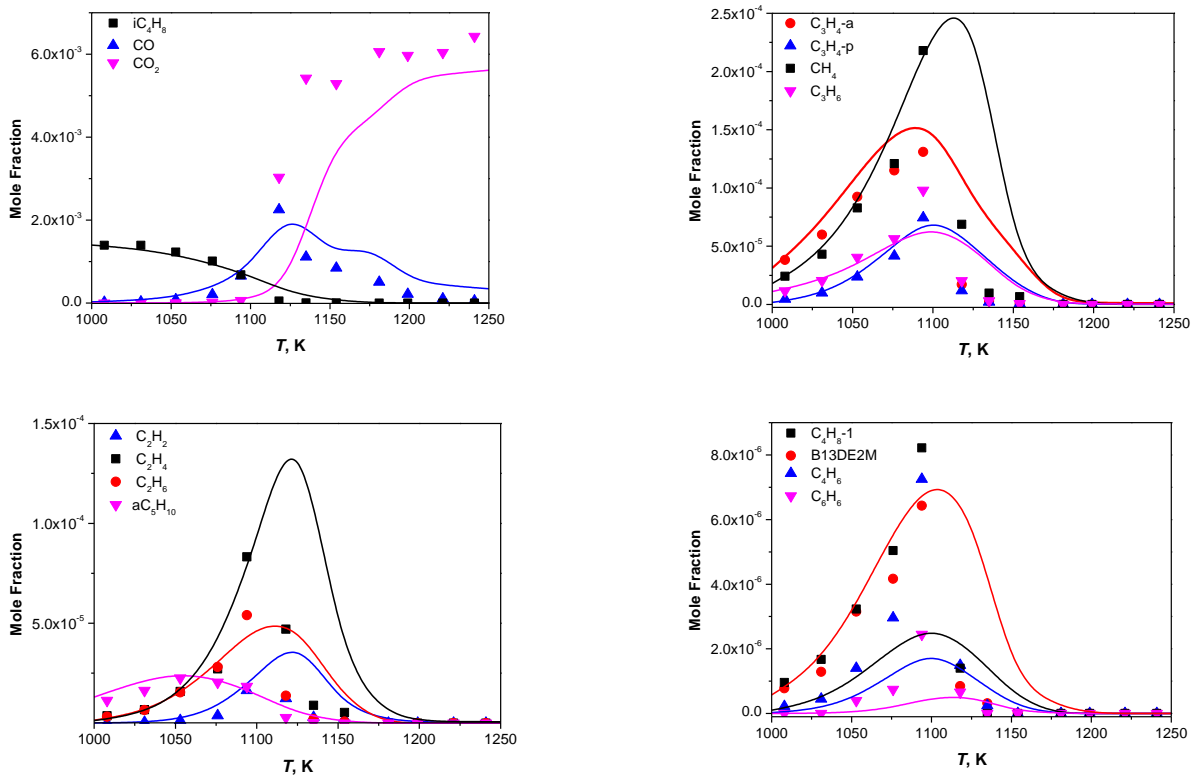
Figure 28. 0.15% iC_4H_8, 4.5% O_2, 95.35% N_2, $\phi = 0.2$, $p = 1$ atm, $\tau = 0.15$ s. Symbols: JSR experimental measurements, lines: current mechanism predictions.
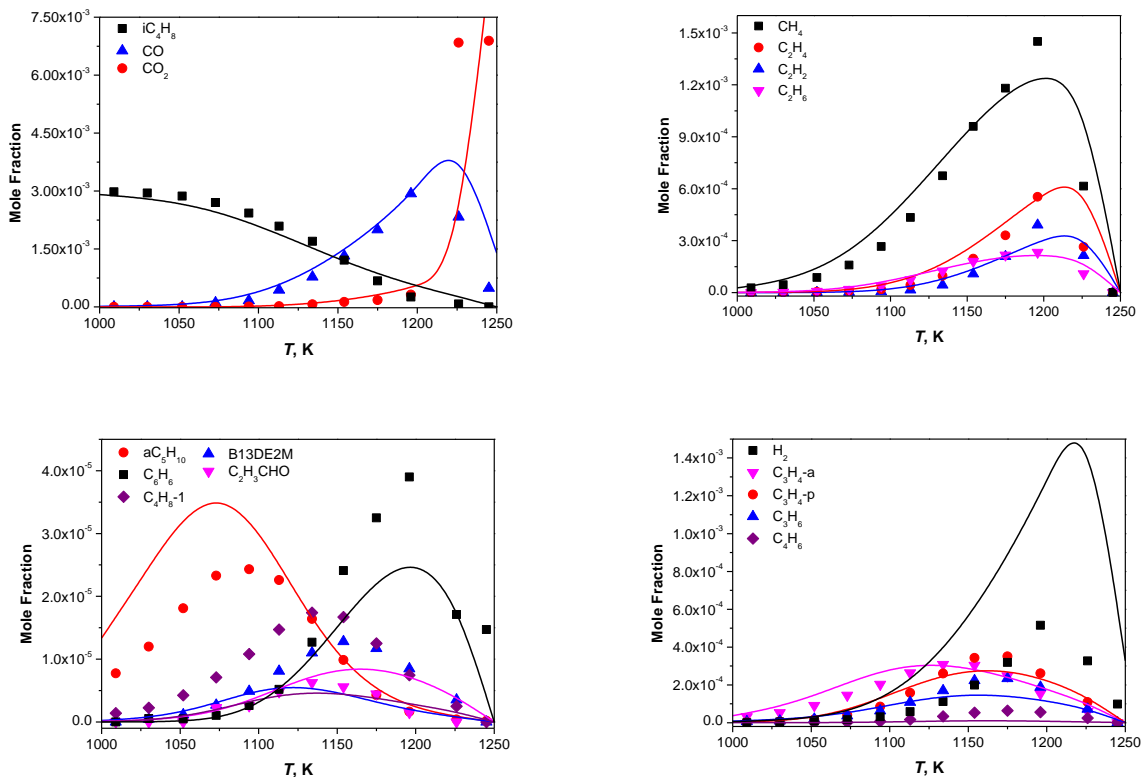

Figure 29. 0.3% iC_4H_8, 1.8% O_2, 97.9% N_2, $\phi = 1.0$, $p = 1$ atm, $\tau = 0.15$ s. Symbols: JSR experimental measurements, lines: current mechanism predictions.
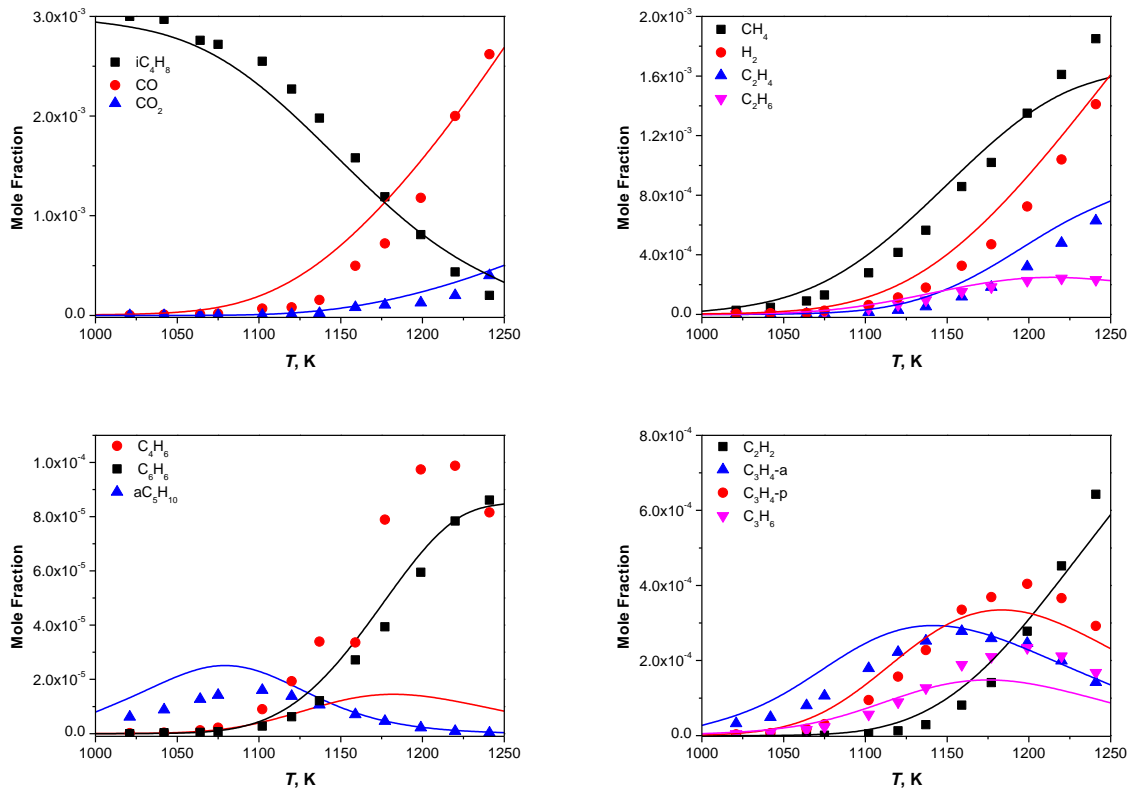
Figure 30. 0.3% iC$_4$H$_8$, 0.9% O$_2$, 98.8% N$_2$, ϕ = 2.0, p = 1 atm, τ = 0.15 s. Symbols: JSR experimental measurements, lines: current mechanism predictions.

Figure 31. 0.15% iC$_4$H$_8$, 0.9% O$_2$, 98.95% N$_2$, ϕ = 1.0, p = 5 atm, τ = 0.75 s. Symbols: JSR experimental measurements, lines: current mechanism predictions.

35

Figure 32. 0.15% iC_4H_8, 4.5% O_2, 95.35% N_2, $\phi = 0.2$, $p = 10$ atm, $\tau = 1.5$ s. Symbols: JSR experimental measurements, lines: current mechanism predictions.

Figure 33. 0.15% iC_4H_8, 0.9% O_2, 98.95% N_2, $\phi = 1.0$, $p = 10$ atm, $\tau = 1.5$ s. Symbols: JSR experimental measurements, lines: current mechanism predictions.
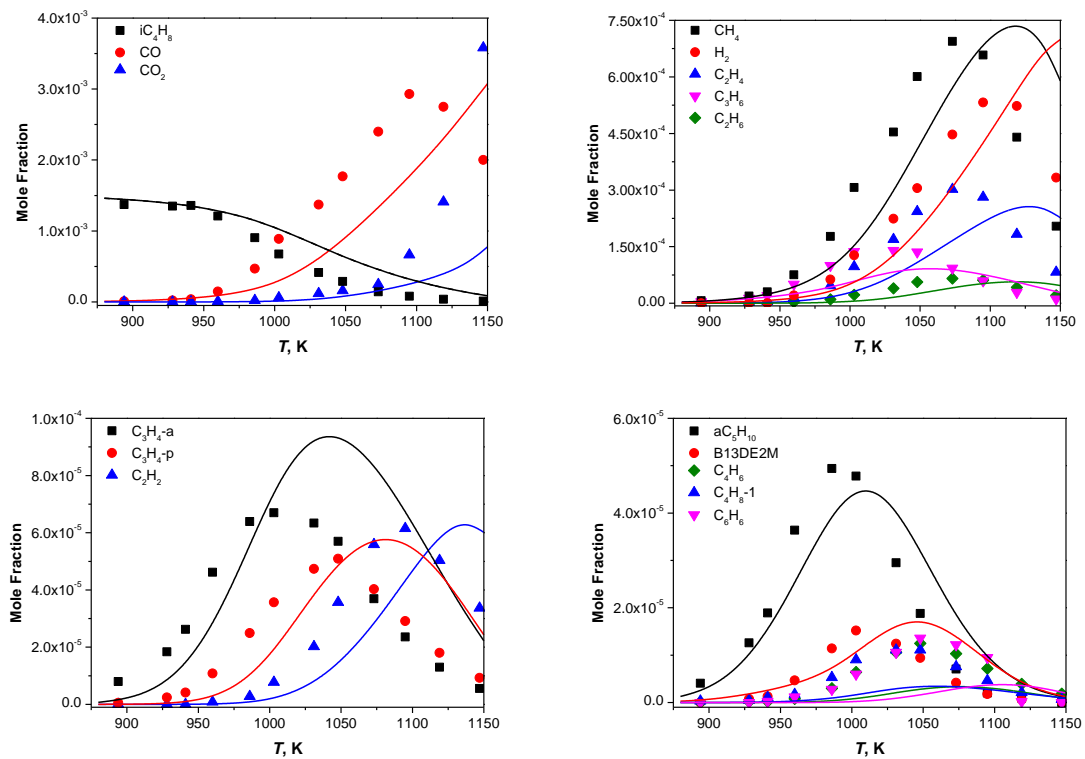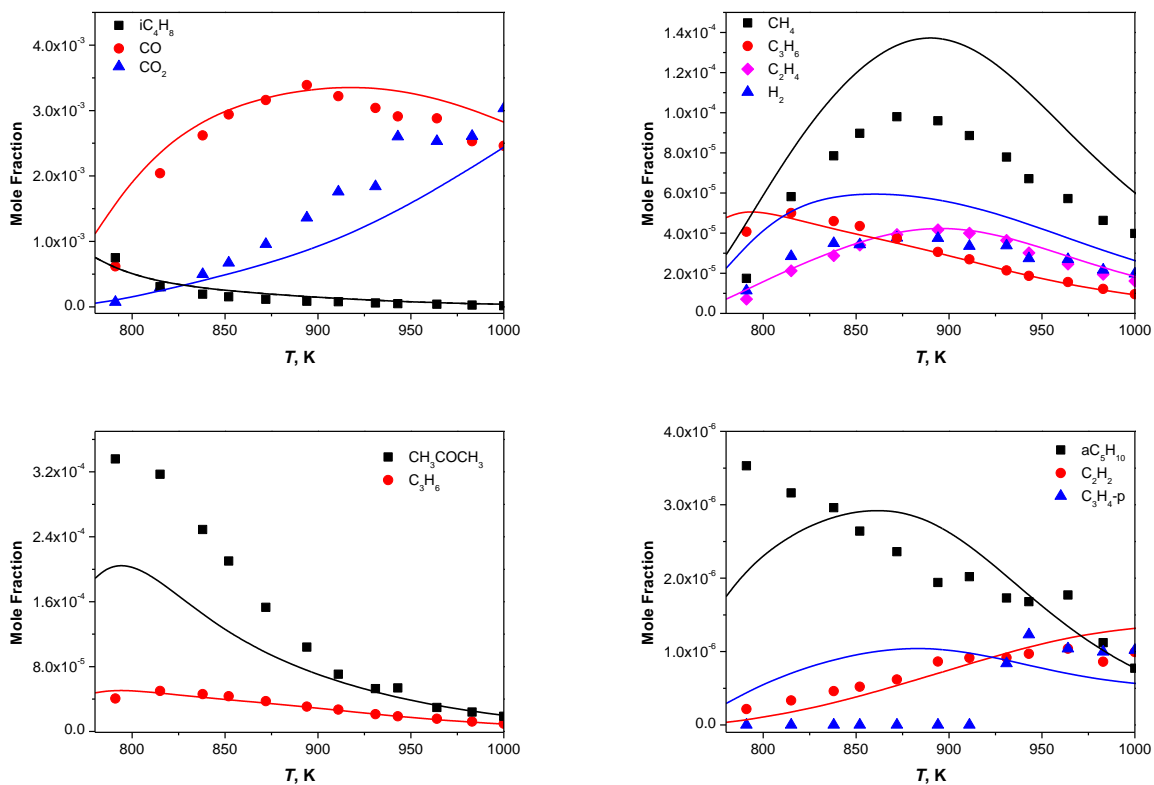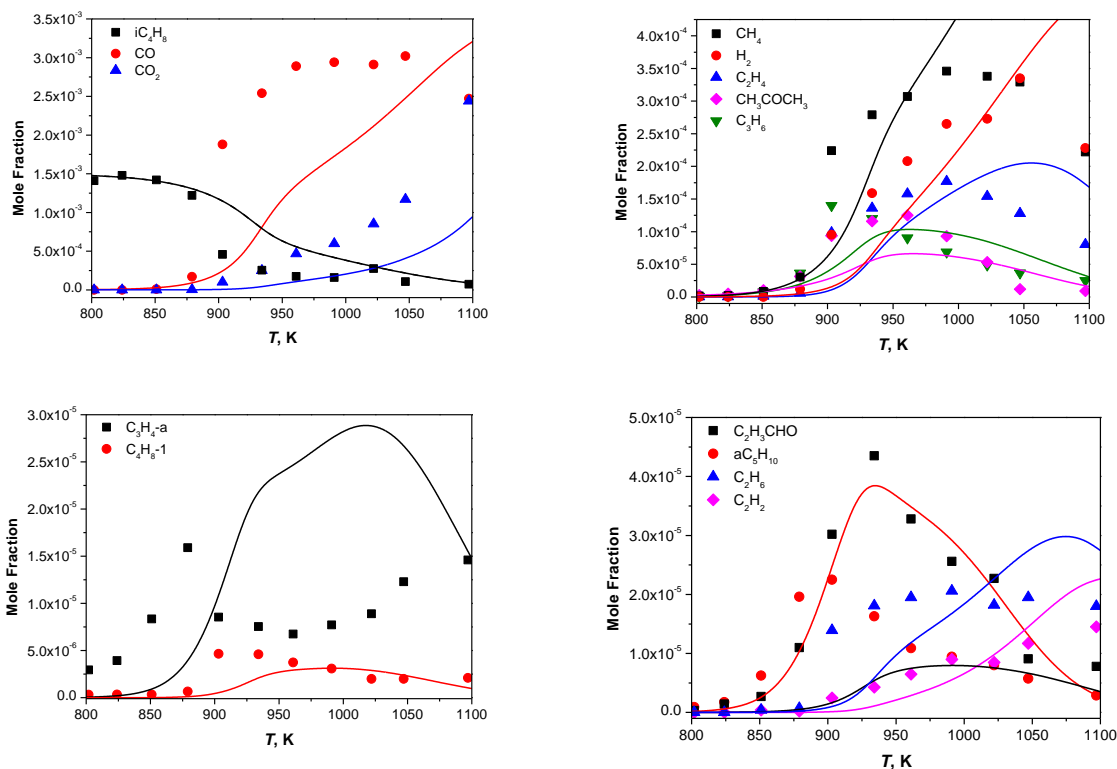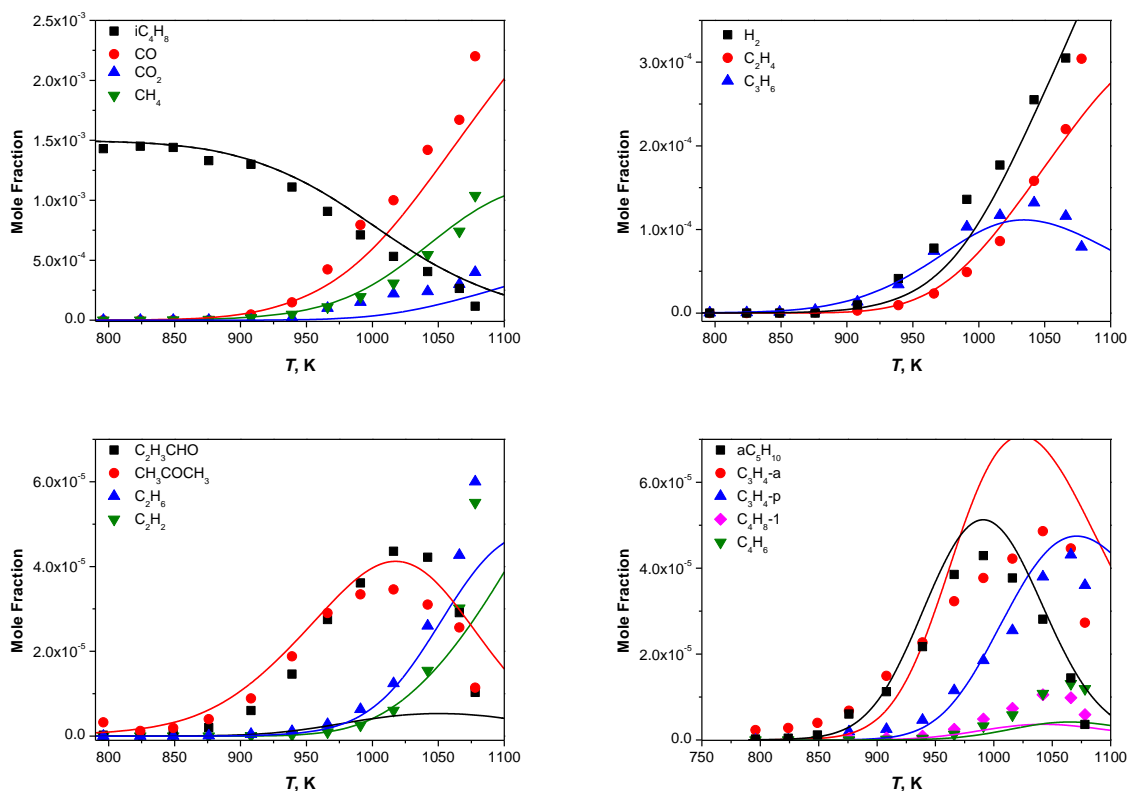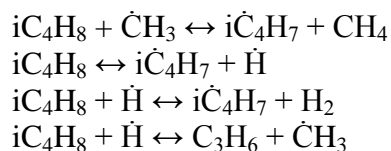
Figure 34. 0.15% iC_4H_8, 0.45% O_2, 99.4% N_2, $\phi = 2.0$, $p = 10$ atm, $\tau = 1.5$ s. Symbols: JSR experimental measurements, lines: current mechanism predictions.

5.4.2 Princeton Atmospheric Pressure Flow reactor (APFR)

Dryer and coworkers [43] have experimentally studied the 1 atm pyrolysis and oxidation of isobutene in the Princeton APFR at initial reaction temperatures of 1081 K and 1139–1150 K. chemical dynamics in the APFR can be simulated using a zero-dimensional, constant pressure adiabatic assumption and a relative time shift between simulation and experimental time. The time-shifting technique has been thoroughly discussed by Dryer et al. [62, 63]. Results for C_3H_4 reported for these experiments and their corresponding simulations are for the sum of allene and propyne.

The single APFR isobutene pyrolysis speciation experiment from [43] provides an important test of isobutene destruction pathways that may otherwise be overwhelmed in the oxidizing experimental environments discussed previously. In hierarchical kinetic model construction, accurate description of pyrolytic pathways is prerequisite for developing accurate oxidation chemistry, and such an approach does much to rule out compensatory uncertainties in both the pyrolysis and oxidation sub-mechanisms. As shown in Figure 35, the present kinetic model generally predicts well the experimentally measured major and minor species profiles. At these conditions, the model indicates that fuel destruction flux is primarily due to the following four reactions:

$$iC_4H_8 + \dot{C}H_3 \leftrightarrow i\dot{C}_4H_7 + CH_4$$
$$iC_4H_8 \leftrightarrow i\dot{C}_4H_7 + \dot{H}$$
$$iC_4H_8 + \dot{H} \leftrightarrow i\dot{C}_4H_7 + H_2$$
$$iC_4H_8 + \dot{H} \leftrightarrow C_3H_6 + \dot{C}H_3$$

Subsequent decomposition of $i\dot{C}_4H_7$ generated in these reactions forms $\dot{C}H_3$ and C_3H_4-a. Consequently, each of the iC_4H_8, CH_4, C_3H_4-a, and C_3H_6 species evolution profiles provides important constraint for these fuel-related reactions. The relatively abundant pool of $\dot{C}H_3$ formed during fuel

destruction may undergo self-recombination to form C_2H_6, which subsequently pyrolyzes to C_2H_4 and then C_2H_2. Though the chemistry subsequent to $\dot{C}H_3$ self-recombination is secondary to the main fuel destruction pathways, its accurate description is critical for prediction of the $\dot{C}H_3$ pool, which is a central driver of the overall fuel decomposition process.

Figure 36Figure 37Figure 38 consider isobutene oxidation at 1 atm. In each of these cases, the isobutene pyrolysis sub-mechanism remains relatively important, despite the oxidizing environment. At 1081 K, very little CO or CO_2 was observed experimentally [11], and the present kinetic model predicts similar rates for $\dot{C}H_3$ and $\dot{O}H$ abstraction of $\dot{H}$ atom from iC_4H_8. At this condition, the present model predicts well each of the iC_4H_8, CH_4, C_3H_6, and C_2H_6 species evolution profiles. However, it over-predicts the formation of C_3H_4 species by a factor of ~1.8. The main fuel destruction flux passes through $i\dot{C}_4H_7$ radicals, and given the central role of these radicals decomposition in populating the $\dot{C}H_3$ pool (and hence the CH_4 and C_2H_6 pools), it is unlikely that the predicted formation rate of C_3H_4-a from $i\dot{C}_4H_7$ radicals is the cause of this discrepancy. This suggests there is either a model deficiency in the overall rate of consumption of C_3H_4-a, or there are problems with the chemistry of C_3H_4-p production and/or destruction. Unfortunately, the ambiguity associated with the lumped C_3H_4 isomer measurement frustrates us in drawing a definitive conclusion. Similar additional C_3H_4 isomer-resolved experiments are clearly desirable to reconcile the noted discrepancy; however, these are beyond the scope of the present work.
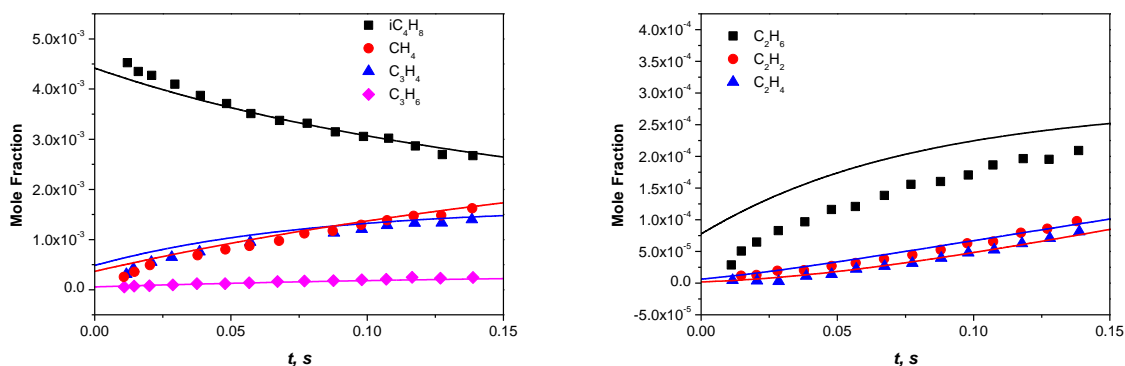

Figure 35. 0.503% iC_4H_8, in N_2, p = 1 atm, T = 1150 K. Symbols: APFR experimental measurements, lines: current mechanism predictions, time shift: –0.26 s.
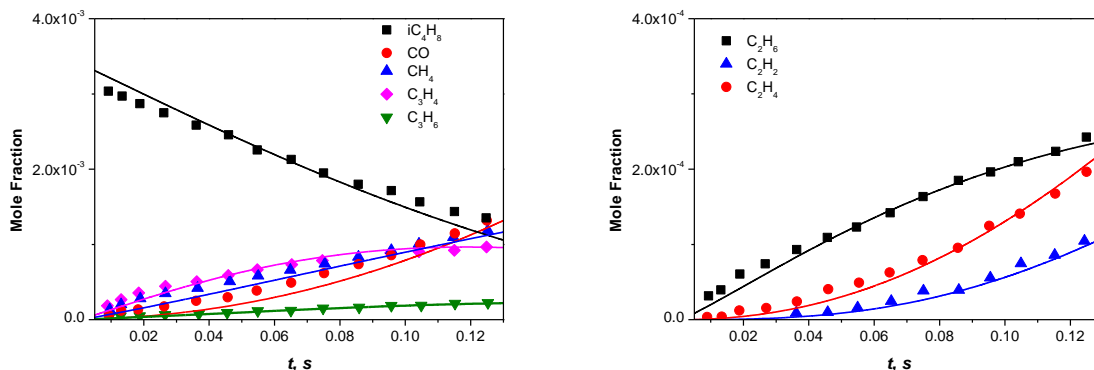

Figure 36. 0.34% iC_4H_8, 2.242% O_2 in N_2, ϕ = 0.91, p = 1 atm, T = 1140 K. Symbols: APFR experimental measurements, lines: current mechanism predictions, time shift: –0.01 s.

Figure 37. 0.348% iC$_4$H$_8$, 1.619% O$_2$ in N$_2$, ϕ = 1.29, p = 1 atm, T = 1142 K. Symbols: APFR experimental measurements, lines: current mechanism predictions, time shift: –0.02 s.

Figure 38. 0.333% iC$_4$H$_8$, 4.757% O$_2$ in N$_2$, ϕ = 0.42, p = 1 atm, T = 1139 K. Symbols: APFR experimental measurements, lines: current mechanism predictions, time shift: 0.01 s.
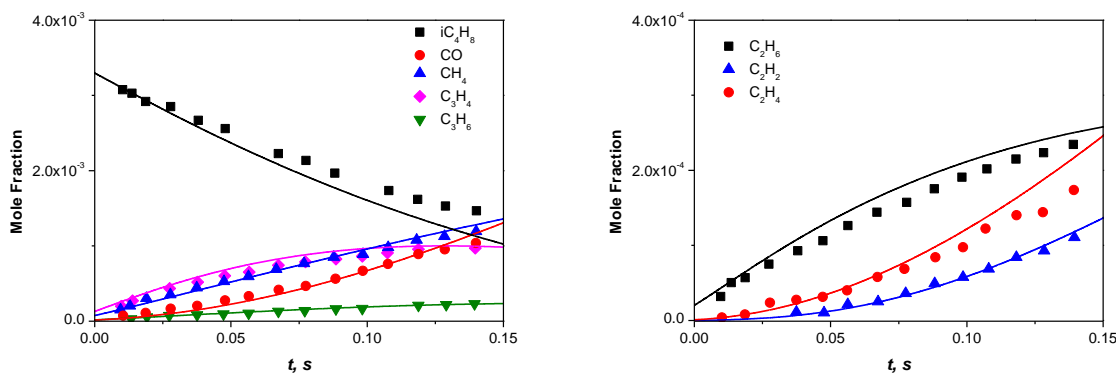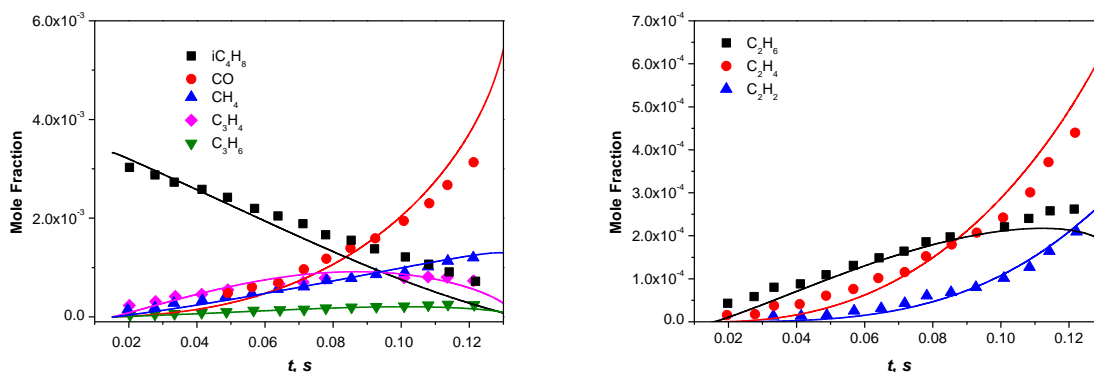
6. Conclusions

This paper presents novel experiments on the ignition delay time and flame speed measurements of isobutene. We also describe the development of a detailed kinetic mechanism which is based on a combination of literature theoretical studies, newly presented *ab initio* calculations and estimates by analogy with propene chemistry. The kinetic model includes comprehensive low- and high-temperature reaction pathways specific to unsaturated fuel chemistry. The mechanism is validated against our new experiments and relevant literature data with sensitivity and flux analyses used to identify important reaction pathways and kinetic parameters. The current mechanism captures most of the experimental results of ignition delay times and flame speeds quite well and also the speciation results from jet-stirred reactor and flow reactor results from the literature.

H-atom abstraction from isobutene by hydroxyl radicals significantly inhibits reactivity through the entire temperature and pressure range investigated because the reaction consumes very reactive hydroxyl radical to produce unreactive stabilized 2-methyallyl radical. H-atom abstraction from isobutene by molecular oxygen to form 2-methyallyl and hydroperoxyl radicals (iC$_4$H$_8$ + O$_2$ ↔ iĊ$_4$H$_7$ + HȮ$_2$) inhibits reactivity at lower temperatures (< 900 K) because, at these temperatures, the reaction proceeds in the reverse direction. This reaction promotes reactivity as the temperature increases and contributes significantly to the reactivity at higher temperatures for all mixtures. Its contribution to the reactivity is significant even at intermediate temperatures (~900 K) under fuel-rich conditions.

At low temperatures (~750 K), $\dot{O}H$ radical additions to iC_4H_8 are very important pathways for fuel consumption and contribute significantly to the overall reactivity. At intermediate temperatures (850 – 1000 K), the reaction of 2-methylallyl ($i\dot{C}_4H_7$) and hydroperoxyl radicals and $i\dot{C}_4H_7$ self-recombination control reactivity. At higher temperatures (~1250 K), the reaction of $i\dot{C}_4H_7$ radicals with $\dot{C}H_3$ radicals becomes important.

JSR speciation predictions were shown to be in reasonable agreement with literature experimental data for equivalence ratios from 0.2 to 2, temperatures of 800–1240 K and the pressures from 1 to 10 atm. The product of the 2-methylallyl radical self-recombination reaction, H15DE25DM, is a very important intermediate species which was not reported in the JSR results. Methacrolein, formed through the decomposition of the methyl-allyoxyl radical, is also an important intermediate which is absent from the JSR results. Future speciation experiments, especially for these species, will be helpful to improve the model. Model predictions for flow reactor speciation were shown to be in reasonable agreement with available literature data as well.

7. Research outlook

Isobutene combustion chemistry is very important in describing the combustion behavior of larger alkanes, as well as being a component of commercial fuels. Despite the fact that the current model accurately captures a wide range of reactivity and speciation results, further fundamental research can aid the important process in improving the accuracy and mechanistic realism of future models. The present study highlights many issues concerning the detailed chemical mechanism development of isobutene combustion, and we summarize these important aspects and present a foundation for future unsaturated alkene combustion mechanism generation.

- The *ab initio* calculation methods applied in this paper provide very good results for the H-atom abstraction reactions of $iC_4H_8 + \dot{O}H$, and $iC_4H_8 + H\dot{O}_2$ which are very important in the entire temperatures and also for the uni-molecular decomposition reaction of $i\dot{C}_4H_7$ radical which is important in the higher temperatures.

- Application of the analogous rate constants for isobutene based on propene for similar reaction classes appears to provide reasonable results for the reaction of $i\dot{C}_4H_7 + H\dot{O}_2$ and $i\dot{C}_4H_7 + i\dot{C}_4H_7$ which are very important at intermediate temperatures. Further *ab initio* calculations and experiments are needed to test the accuracy of the rate constants estimated by analogy.

- The H-atom abstraction rate constant from iC_4H_8 by molecular oxygen is different from the analogous reaction in propene. As this reaction in the current form results in good predictions of ignition delay times in fuel-rich mixtures, we use the current value. *Ab initio* calculations for this reaction class in both the propene and isobutene systems are needed in order to improve the fidelity of the model.

- After the fuel radical $\dot{R}$ reacts with molecular oxygen to form $R\dot{O}_2$, this radical then decomposes back to $\dot{R} + O_2$ in unsaturated alkenes, while $R\dot{O}_2$ is more stable for normal alkanes. Based on this work, and related studies of allylic systems, it is becoming apparent that the reactivity for alkene components at very low temperatures (< 800 K) is from the hydroxyl radical addition reaction followed by addition of the resulting radical to molecular oxygen. At intermediate temperatures (800–1300 K), the reactivity is controlled by the competition between hydrogen abstractions by molecular oxygen and $\dot{O}H$ radicals from alkenes and the reaction between resonantly stabilized $i\dot{C}_4H_7$ radical reacting with hydroperoxyl radicals resulting in chain branching reactions. At higher temperatures (> 1300 K), the reactivity is mainly from the hydrogen abstraction reactions from the fuel by molecular oxygen.

- Our current treatment captures the low temperature reactivity of isobutene oxidation well; while further fundamental research studies to provide accurate pressure and temperature dependence rate constants for the first and second addition to molecular oxygen reactions are needed to give a better understanding of the low temperature chemistry of alkene fuel oxidation.

- For our future modeling studies of 1-butene, 2-butene and 1,3-butadiene, the following reaction classes need to be accurately described: H-atom abstraction by $\dot{O}H$, $H\dot{O}_2$ radicals and molecule oxygen from fuel molecules; the radical recombination reactions between $\dot{R}$ and $H\dot{O}_2$, $\dot{C}H_3$, and $\dot{R}$ radicals; the decomposition reaction of $\dot{R}$ radical; the addition reactions of $\dot{H}$ atom, $\dot{O}H$ and $H\dot{O}_2$ radicals to fuel molecules. Experimental and theoretical investigations on those reaction classes are important in reveal the combustion chemistry of those fuels.

The present chemical mechanism study of the isobutene oxidation provides a comprehensive methodology to develop similar models for unsaturated alkenes, such as 1-butene, 2-butene and 1,3-butadine. In addition, this work provides an important sub-mechanism for transportation fuels

combustion modeling. The combustion chemistry features that distinguish the unsaturated alkenes from their branched alkane relatives highlighted in this work are also very interesting. We hope the remaining challenges presented in this final section will motivate theoreticians and experimentalists to discover additional uncertainties of the kinetics properties of important reaction classes for the unsaturated alkenes combustion chemistry.

References

1. C. K. Westbrook; W. J. Pitz; H. J. Curran, J. Phys. Chem. A 110 (21) (2006) 6912-6922.
2. S. M. Burke; U. Burke; R. Mc Donagh; O. Mathieu; I. Osorio; C. Keesee; A. Morones; E. L. Petersen; W. J. Wang; T. A. DeVerter; M. A. Oehlschlaeger; B. Rhodes; R. K. Hanson; D. F. Davidson; B. W. Weber; C. J. Sung; J. Santner; Y. G. Ju; F. M. Haas; F. L. Dryer; E. N. Volkov; E. J. K. Nilsson; A. A. Konnov; M. Alrefae; F. Khaled; A. Farooq; P. Dirrenberger; P. A. Glaude; F. Battin-Leclerc; H. J. Curran, Combust. Flame 162 (2) (2015) 296-314.
3. S. M. Burke; W. Metcalfe; O. Herbinet; F. Battin-Leclerc; F. M. Haas; J. Santner; F. L. Dryer; H. J. Curran, Combust. Flame 161 (11) (2014) 2765-2784.
4. J. C. Bauge; F. Battin-Leclerc; F. Baronnet, International Journal of Chemical Kinetics 30 (9) (1998) 629-640.
5. J. N. Bradley; K. O. West, Journal of the Chemical Society-Faraday Transactions I 72 (1976) 558-567.
6. H. J. Curran; M. P. Dunphy; J. M. Simmie; C. K. Westbrook; W. J. Pitz, Symposium (International) on Combustion 24 (1) (1992) 769-776.
7. S. Santhanam; J. H. Kiefer; R. S. Tranter; N. K. Srinivasan, Int. J. Chem. Kinet. 35 (8) (2003) 381-390.
8. W. Tsang; J. A. Walker, Symposium (International) on Combustion 22 (1) (1989) 1015-1022.
9. K. Yasunaga; Y. Kuraguchi; R. Ikeuchi; H. Masaoka; O. Takahashi; T. Koike; Y. Hidaka, Proc. Combust. Inst. 32 (2009) 453-460.
10. H. J. Curran, PhD Thesis, Department of Chemistry, University College, Galway. (1994)
11. K. Brezinsky; F. L. Dryer, Combust. Sci. Technol. 45 (5-6) (1986) 225-232.
12. P. Dagaut; M. Cathonnet, Combust. Sci. Technol. 137 (1-6) (1998) 237-275.
13. V. Dias; J. Vandooren, Fuel 89 (9) (2010) 2633-2639.
14. M. Schenk; L. Leon; K. Moshammer; P. Osswald; T. Zeuch; L. Seidel; F. Mauss; K. Kohse-Hoinghaus, Combust. Flame 160 (3) (2013) 487-503.
15. P. Zhao; W. H. Yuan; H. Y. Sun; Y. Y. Li; A. P. Kelley; X. L. Zheng; C. K. Law, Proc. Combust. Inst. 35 (2015) 309-316.
16. Y. J. Zhang; J. H. Cai; L. Zhao; J. Z. Yang; H. F. Jin; Z. J. Cheng; Y. Y. Li; L. D. Zhang; F. Qi, Combust. Flame 159 (3) (2012) 905-917.
17. J. H. Cai; L. D. Zhang; F. Zhang; Z. D. Wang; Z. J. Cheng; W. H. Yuan; F. Qi, Energy Fuels 26 (9) (2012) 5550-5568.
18. C. J. Aul; W. K. Metcalfe; S. M. Burke; H. J. Curran; E. L. Petersen, Combust. Flame 160 (7) (2013) 1153-1167.
19. H. P. S. Shen; J. Vanderover; M. A. Oehlschlaeger, Combust. Flame 155 (4) (2008) 739-755.
20. A. K. Das; C. J. Sung; Y. Zhang; G. Mittal, Int. J. Hydrog. Energy 37 (8) (2012) 6901-6911.
21. J. M. Hall; E. L. Petersen, Int. J. Chem. Kinet. 38 (12) (2006) 714-724.
22. T. Kathrotia; M. Fikri; M. Bozkurt; M. Hartmann; U. Riedel; C. Schulz, Combust. Flame 157 (7) (2010) 1261-1273.
23. C. K. Westbrook; W. J. Pitz; J. E. Boercker; H. J. Curran; J. F. Griffiths; C. Mohamed; M. Ribaucour, Proceedings of the Combustion Institute 29 (1) (2002) 1311-1318.
24. S. Tanaka; F. Ayala; J. C. Keck, Combustion and Flame 133 (4) (2003) 467-481.
25. M. Ribaucour; R. Minetti; L. R. Sochet; H. J. Curran; W. J. Pitz; C. K. Westbrook, Proceedings of the Combustion Institute 28 (2) (2000) 1671-1678.
26. v. CHEMKIN-PRO, Reaction Design: San Diego, 2013.)
27. M. C. Krejci; O. Mathieu; A. J. Vissotski; S. Ravi; T. G. Sikes; E. L. Petersen; A. Kermones; W. Metcalfe; H. J. Curran, J. Eng. Gas. Turbines Power-Trans. ASME 135 (2) (2013) 9.
28. Z. Chen, Combustion and Flame 158 (2) (2011) 291-300.
29. X. Qin; Y. Ju, Proceedings of the Combustion Institute 30 (1) (2005) 233-240.
30. P. Dirrenberger; H. Le Gall; R. Bounaceur; O. Herbinet; P. A. Glaude; A. Konnov; F. Battin-Leclerc, Energy Fuels 25 (9) (2011) 3875-3884.
31. P. Dirrenberger; P. A. Glaude; R. Bounaceur; H. Le Gall; A. P. da Cruz; A. A. Konnov; F. Battin-Leclerc, Fuel 115 (2014) 162-169.
32. P. Dirrenberger; H. Le Gall; R. Bounaceur; P. A. Glaude; F. Battin-Leclerc, Energy Fuels 29 (1) (2015) 398-404.
33. W. K. Metcalfe; S. M. Burke; S. S. Ahmed; H. J. Curran, Int. J. Chem. Kinet. 45 (10) (2013) 638-675.
34. Y. Zhao; D. G. Truhlar, Theor. Chem. Acc. 120 (1-3) (2008) 215-241.
35. M. J. e. a. Frisch, (2009)
36. J. M. L. Martin, Chem. Phys. Lett. 259 (5-6) (1996) 669-678.
37. D. Feller; D. A. Dixon, J. Chem. Phys. 115 (8) (2001) 3484-3496.
38. S. Glasstone; K. J. Laidler; H. Eyring, (1941)
39. C. Eckart, Phys. Rev. 35 (1930) 1303-1309.

40.   K. S. Pitzer; W. D. Gwinn, J. Chem. Phys 10 (1942) 428-440.
41.   A. Keromnes; W. K. Metcalfe; K. A. Heufer; N. Donohoe; A. K. Das; C. J. Sung; J. Herzler; C. Naumann; P. Griebel; O. Mathieu; M. C. Krejci; E. L. Petersen; W. J. Pitz; H. J. Curran, Combust. Flame 160 (6) (2013) 995-1011.
42.   W. Tsang, Journal of Physical and Chemical Reference Data 20 (2) (1991) 221-273.
43.   T. Held; F. L. Dryer, PhD Thesis, Department of Mechanical and Aerospace Engineering, Princeton University. (1993)
44.   H. Y. Sun; C. K. Law, J. Phys. Chem. A 114 (45) (2010) 12088-12098.
45.   J. Zador; A. W. Jasper; J. A. Miller, Phys. Chem. Chem. Phys. 11 (46) (2009) 11040-11053.
46.   H. Y. Sun; J. W. Bozzelli; C. K. Law, J. Phys. Chem. A 111 (23) (2007) 4974-4986.
47.   S. M. Villano; L. K. Huynh; H. H. Carstensen; A. M. Dean, J. Phys. Chem. A 116 (21) (2012) 5068-5089.
48.   A. Miyoshi, Int. J. Chem. Kinet. 44 (1) (2012) 59-74.
49.   C. F. Goldsmith; W. H. Green; S. J. Klippenstein, J. Phys. Chem. A 116 (13) (2012) 3325-3346.
50.   H. J. Curran, Int. J. Chem. Kinet. 38 (4) (2006) 250-275.
51.   J. A. Miller; S. J. Klippenstein, J. Phys. Chem. A 117 (13) (2013) 2718-2727.
52.   J. Zador; S. J. Klippenstein; J. A. Miller, J. Phys. Chem. A 115 (36) (2011) 10218-10225.
53.   S. M. Villano; L. K. Huynh; H. H. Carstensen; A. M. Dean, J. Phys. Chem. A 115 (46) (2011) 13425-13442.
54.   S. M. Villano; H. H. Carstensen; A. M. Dean, J. Phys. Chem. A 117 (30) (2013) 6458-6473.
55.   T. Ingham; R. W. Walker; R. E. Woolford, Symposium (International) on Combustion 25 (1) (1994) 767-774.
56.   C. J. Chen; J. W. Bozzelli, J. Phys. Chem. A 104 (43) (2000) 9715-9732.
57.   C. F. Goldsmith; S. J. Klippenstein; W. H. Green, Proc. Combust. Inst. 33 (2011) 273-282.
58.   S. Rolland; J. M. Simmie, Int. J. Chem. Kinet. 37 (3) (2005) 119-125.
59.   T. W, J. Phys. Chem. Ref. Data 20 (1991)
60.   J. Mendes; C. W. Zhou; H. J. Curran, J. Phys. Chem. A 118 (51) (2014) 12089-12104.
61.   A. Fridlyand; P. T. Lynch; R. S. Tranter; K. Brezinsky, J. Phys. Chem. A 117 (23) (2013) 4762-4776.
62.   Z. Zhao; M. Chaos; A. Kazakov; F. L. Dryer, Int. J. Chem. Kinet. 40 (1) (2008) 1-18.
63.   F. L. Dryer; F. M. Haas; J. Santner; T. I. Farouk; M. Chaos, Progress in Energy and Combustion Science 44 (2014) 19-39.